DIVERTOR TOKAMAK ASDEX

The ASDEX Group

IPP III/47 November 1978

MAX-PLANCK-INSTITUT FÜR PLASMAPHYSIK

8046 GARCHING BEI MÜNCHEN

MAX-PLANCK-INSTITUT FÜR PLASMAPHYSIK

GARCHING BEI MÜNCHEN

DIVERTOR TOKAMAK ASDEX

The ASDEX Group

IPP III/47 November 1978

Die nachstehende Arbeit wurde im Rahmen des Vertrages zwischen dem Max-Planck-Institut für Plasmaphysik und der Europäischen Atomgemeinschaft über die Zusammenarbeit auf dem Gebiete der Plasmaphysik durchgeführt.

IPP III/47 The ASDEX Group DIVERTOR TOKAMAK ASDEX

Preface

Like the previous report "Divertor Tokamak ASDEX" from July 1976 (IPP III/27) this report is intended to summarize information on the design and construction of ASDEX. It compiles 7 papers presented by the ASDEX Group at the

6th International Conference on Magnet Technology, Bratislava, CSR (29.8.-2.9.1977) and the

10th Symposium on Fusion Technology, Padua, Italy (4.-8.9.1978)

The first paper

reports on the assembly and testing of the toroidal field and Ohmic heating coils and on the status of the other components.

The remaining 6 papers describe special components and topics in more detail:

STATUS OF THE ASDEX TOKAMAK

Wesner,F., Allgeyer,R., Broser,E., Finkelmeyer,H.,Franzspeck,J., Gernhardt,J., Gresser,F., Griek,R., Haas,G., Hartz,F., Herppich,G., Jandl,O., Keilhacker,M., Klement,G., Kornherr,M., Kotzlowski,H., Krüger,P.,Larcher,Th.v., Mark,E.v., Niedermeyer,H., Pillsticker,M., Preis,H., Rapp,H., Schneider,F., Wagner,F., Wedler,H., Werner,F.

Abstract

The present status of the ASDEX divertor tokamak and its main components is given. The toroidal field coils and the "inner" poloidal field coils are complete and have largely been tested. The test results are reported. The divertor field coils will be delivered this autumn. The vacuum vessel is being prepared for installation. The design principle and status of the vacuum system, the power supply and the control systems are described.

Introduction

The ASDEX divertor tokamak can be divided into two halves in order to allow installation of the likewise divisible vacuum vessel. All poloidal field coils, being composed of detachable segments, are situated within the toroidal field coils. The "inner" ones of these segmented coils, being situated behind the vacuum vessel, must be joined together when the vessel halves are inserted in the experiment, but before they are closed. The main components of ASDEX are described in detail in /1/ and /2/.

Coil systems

The toroidal field coil system (Fig.1) has already been completed and was tested in May and June 1977 /3/. In these tests it could be shown that the toroidal field coils can be

operated at their full design parameters (45 kA, corresponding to 2.8 T at plasma centre; 5 s flat-top time). The movements and elastic deformations of the windings in their stainless steel casings, which are caused by thermal expansion and magnetic forces, proved to be within tolerable limits and in good agreement with the calculations. The compression rate and the elongation of the central column, effected by the centripetal forces (the coils do not form a vault), agree with the values expected from model tests. The cooling system is able to cool down the windings within 6 minutes, guaranteeing little temperature difference in the windings by programmed reduction of the water temperature.

After completion of the 18 inner OH transformer coils (90 of the 100 turns of the transformer, Fig.2) and of the switching circuit, this system was also tested (see paper IV in this report "Testing and Performance of the 30 kA Ohmic Heating System of ASDEX.

Primarily the following parameters have been measured:
- Currents and voltages of coils and switching circuit
- Coil temperatures
- Movements of coils, current leads and mechanical structures by means of 60 linear potentiometers.

The following parameters were checked by an automatic monitoring system:
- Water flow rate in all cooling circuits
- Symmetry of the voltage drops in the coil systems
- Resistance between the casings of the toroidal field coils and earth
- Movements of the toroidal field windings within their casings
- Compression of the central column
- Current in the transformer coils and possible earth currents of the coils in the case of arcing.

To monitor the critical values of movements and temperatures an electronic monitoring system with 126 channels is used. In connexion with the ASDEX computer (PDP 11/70) it is possible to record and plot the signals.

The measurements showed that both coil systems can be operated at their full design parameters (transformer current 30 kA, corresponding to 2,5 Vs; voltage at current breaking 20 kV). The transformer coils work satisfactorily with respect to their electrical and mechanical characteristics. Deformations, movements and the asymmetry of the movements are tolerable. The switching circuit, including the preliminary air blast breaker, proved to be suitable for the operational parameters of ASDEX, but the electrodes of this breaker have to be exchanged after a few hundred shots.

The other inner poloidal field coils, e.g. vertical field coils, divertor compensating field coils (10 single-turn coils) and two radial field coils (two turns each), will be tested after completion in September 1978 (Fig.3).

The divertor field coils are being manufactured, their delivery being expected in autumn this year.

The design and fabrication of the divisible poloidal field coils was difficult because of the narrow space available for the coils, their turn cross-overs and their current leads and because of the accurate machining necessary for the joints. In the case of the divertor field coils, fabrication difficulties concerning the cross-over parts (beryllium copper castings) resulted in great delay.

Vacuum vessel

The vacuum vessel (Fig.4) was delivered in spring 1977. Subsequently it was heated up to 150° C and successfully leak-tested. In the meantime, the following parts have been fitted into the vacuum vessel: supports to fix the divertor field coils, divertor coil fixtures, divertor chamber separating plates, getter panels belonging to the divertor pumping system, and passive plasma-stabilizing coils. Many built-in diagnostic facilities have also been installed, e.g. electromagnetic probes and loops (see paper J 10), microwave diagnostics, limiter temperature observations and equipment for preionisation.

Vacuum system

ASDEX has a base vacuum system consisting of 8 turbomolecular pumps (pumping speed of each pump 3500 l/s), which is already completed and ready to be installed, and a divertor pumping system.

The divertor pumping system consists of:

- liquid nitrogen cooled getter panels covering the vessel walls in 26 of the 32 divertor chambers (Fig.5). In order to reduce dangerous eddy currents induced by plasma disruptions, the panel plates are composed of many anodized aluminium profiles, electron-beam-welded onto aluminium bars and additionally pressed together by tensile bars.

  The getter panels have partly been delivered and fitted into the vacuum vessel. They will be finally inserted after the divertor field coils have been installed.

- Two titanium sublimators in each of these 26 divertor chambers. Each sublimator consists of two parallel Cu bars onto which 19 titanium-molybdenum wires are clamped (Fig.6). About 0.8 mg

of titanium per pulse and a total of more than 19 g titanium can be evaporated by one sublimator. The 19 wires are directly heated by a current of 750-1000 A, all wires and sublimators being connected in parallel. When a certain number of wires is fused, the sublimators have to be replaced from outside the vacuum vessel. The sublimators are being manufactured at present.

- A liquid-nitrogen cooling and heating system which pumps the nitrogen through the getter panels. It is possible to set each temperature between 80 K and 150° C by pumping pure liquid, mixed liquid-gaseous or heated gaseous nitrogen through the panels. The cooling and heating system is already complete.

  Measurements made with the prototype getter panel in a divertor chamber model showed that this system should be able to pump 50 mbarl H_2 with a pumping speed larger than $2.4 \cdot 10^6$ l/s.

Power supply system

All distribution elements and switchgear to connect the coils with the power supply systems of the institute have been completed. The coil systems are powered by the following generators:

- 1.5 GJ flywheel generator with diode bridge to power the toroidal field coils. Main generator data: 150 MVA,100 cps; DC 45 kA, 10 s, 3.3 kV
- 500 MJ flywheel generator with 10 separate thyristor rectifier modules. Main data: 144 MVA, 100 cps; DC 22.5 kA, 5 s, 1.2 kV per module.

  This generator powers the
  . ohmic heating transformer with feedback control of the flat-top plasma current,
  . vertical field coils with feedback control of the radial plasma position (see paper J10),

. divertor field coils with programmed current.

- 15 MJ flywheel generator with mercury arc rectifiers for alternative powering of the transformer coils
- 4-quadrant transistor amplifier (250 kW) to power the radial field coils (feedback control of vertical plasma position).

Operational modes of the experiment:
The coils of the divertor field triplets can be operated in series, or separately. This enables

- normal or divertor tokamak operation with circular plasma cross-sections
- normal or divertor tokamak operation with eliptical or D-shaped plasma cross-sections.

Control system

The control system of ASDEX is hierarchically organized (Fig.7). It allows common operation of all systems, controlled by the central control unit, as well as separate operation of the components, controlled by their own subcontrol systems (e.g. for first time operation or tests).

The central control unit controls the experimental state and the program by means of commands to the subsystems and auxiliary systems. It provides an interlocking system to protect the machine.

The subcontrol systems are technically autonomous systems to control the components of ASDEX (e.g. toroidal field coils, vacuum systems etc-). All subsystems have an internal interlocking system.

Auxiliary systems are necessary to allow separate operation of some components (e.g. coil systems) without the central control unit. These system have direct contacts to subsystems (direct

contact between two subcontrol systems is not allowed).

The central control unit and some subcontrol and auxiliary systems are complete. The other systems are being manufactured.

References

/1/ Proc.of the 9th Symposium on Fusion Technology, Garmisch-Partenkirchen, 1976
/2/ Proc.of the 6th International Conference on Magnet Technology, Bratislava, 1977
/3/ Proc.7th Symposium on Engineering Problems of Fusion Research, Knoxville, USA, 1977.

Fig.1: Toroidal field coil system, with some of the inner OH transformer coils already installed.

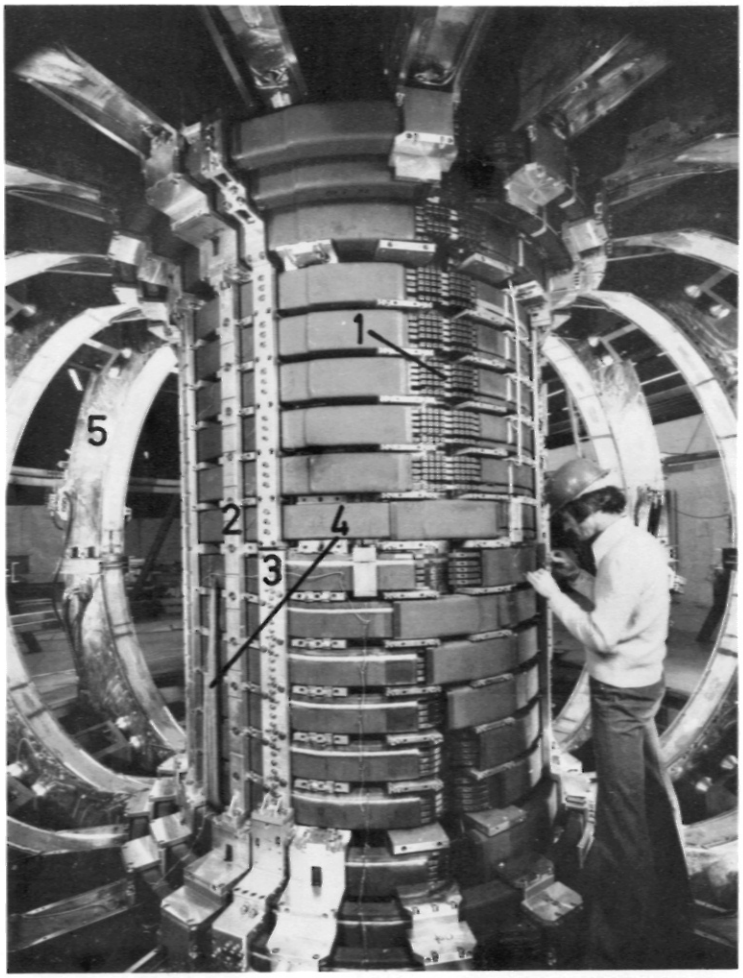

Fig.2: Inner OH transformer coils

1 Joints of the detachable coils

2 Transformer coil fixtures (allowing radial movements)

3 Mutual braces of the transformer coils

4 Cooling water connections

5 Toroidal field coils

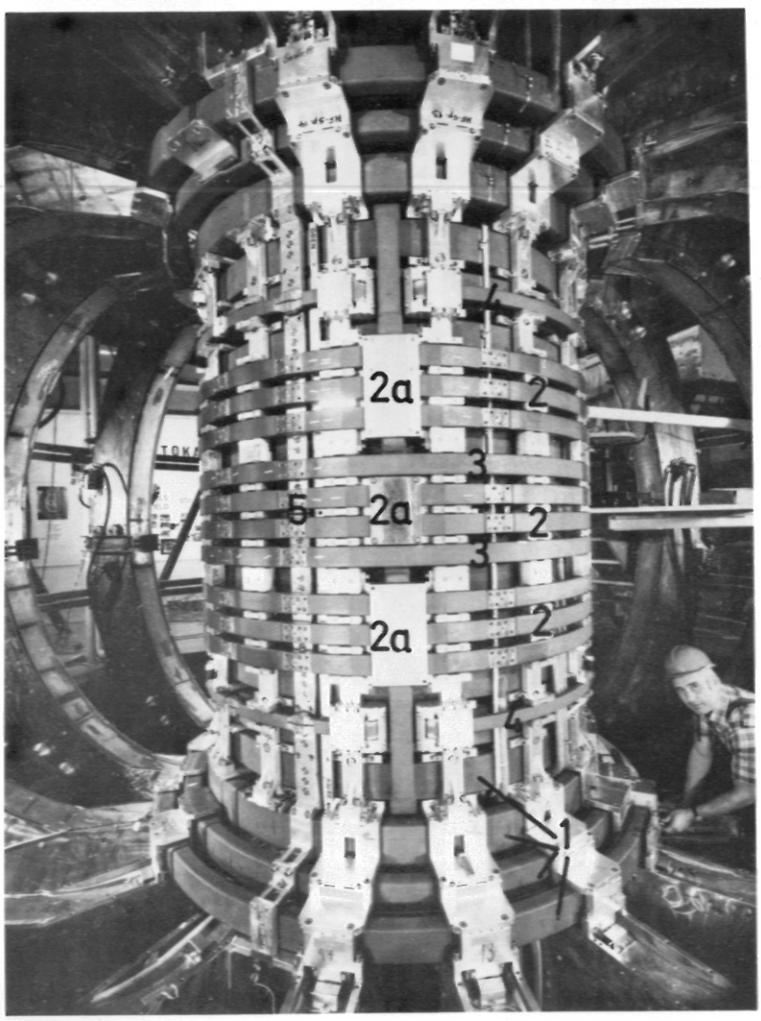

Fig.3: Inner poloidal field coils

1 Transformer coils

2 Vertical field coils

2a Fixture of the turn cross-over section

3 Divertor field compensating coils

4 Radial field coils

5 Joints of the turn segments

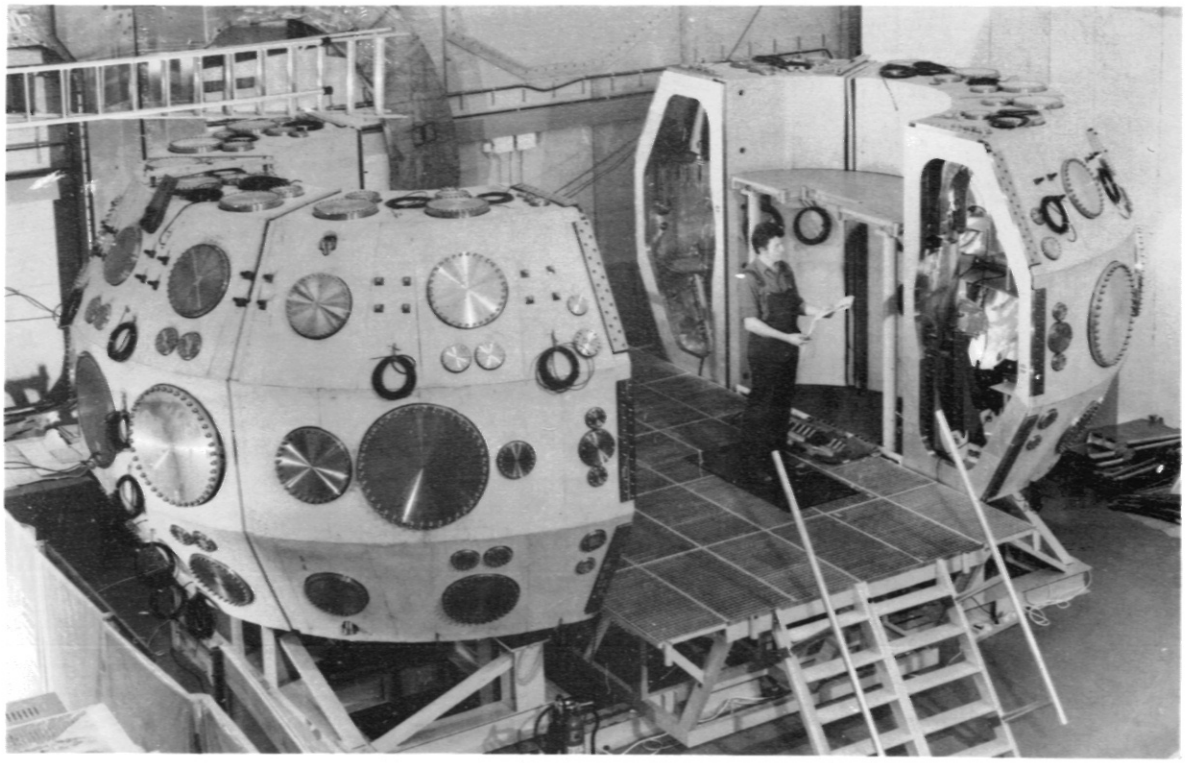

Fig.4: Vakuum vessel halves

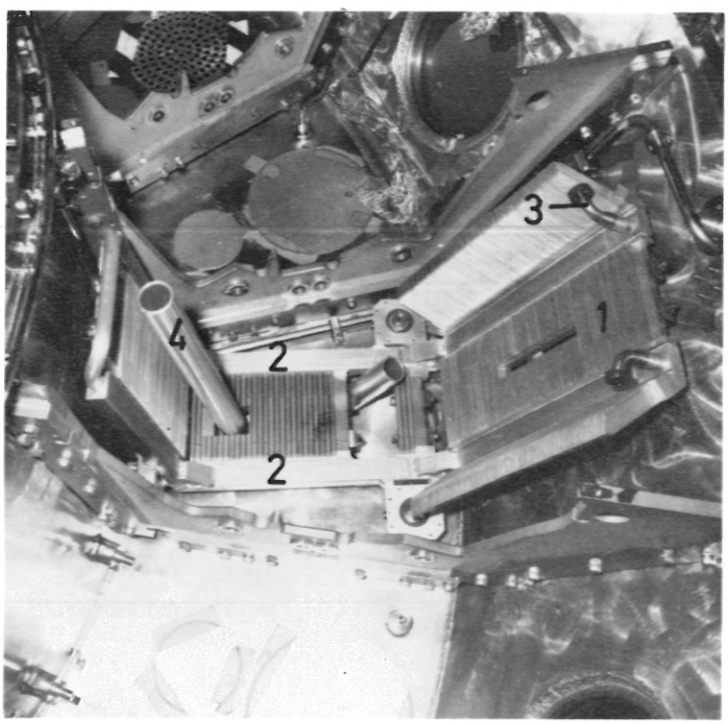

Fig.5: One getter panel of the divertor pumping system, being fitted into the vacuum vessel

1 Aluminium profiles, welded onto aluminium bars (2)

3 Nitrogen inlets and outlets

4 Titanium sublimator dummies

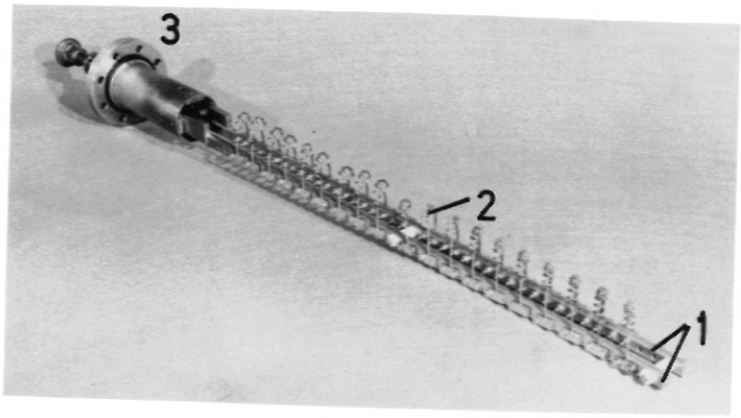

Fig.6: Titanium sublimator
1 Copper bars
2 Titanium molybdenum wires
3 Flange with 1 kA vakuum feed-through

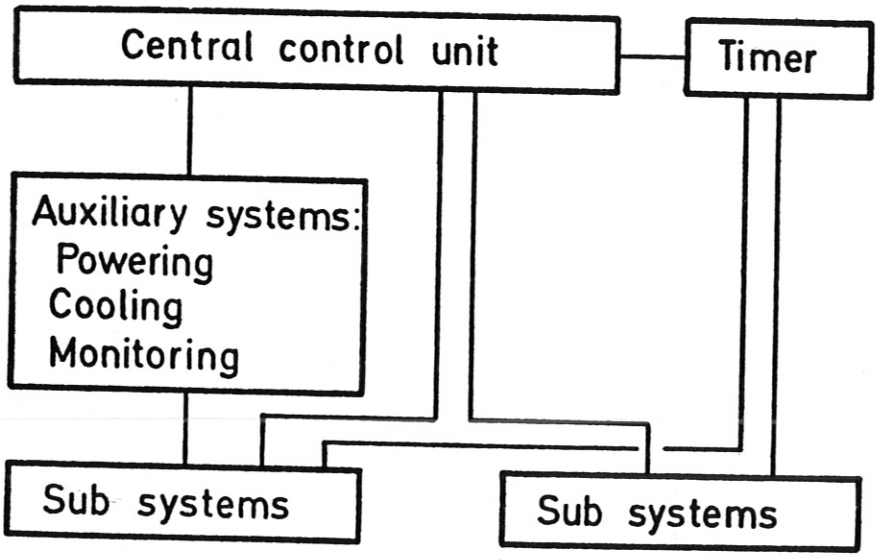

Fig.7: Principle of the ASDEX control system

STRAIN AND STRESS OF THE A S D E X MULTIPOLE MAGNETIC COILS

O. Jandl, M. Pillsticker

Summary

A brief description of the technical concept of the multipole magnetic field coils for the ASDEX tokamak is given. The various loads of the coils are explained in quality. To compute displacement and stress of the coils FEM computer programs are used. The computing models applied to this problem are founded and the results and the conclusions are reported.

Introduction

The two multipole magnetic field coils (MP) triplets of the ASDEX tokamak induce the field for the axisymmetric divertor and the magnetic limiter/1/. The coils must be installed within the vacum vessel near the plasma (Fig. 1). The design chosen imposes high stresses in certain regions of the material. Detailed computations were essential to reduce the safety factor to an acceptable value from the technical point of view.

General technical concept

All coils (Fig. 2) are devided into two halves, which are force- and current-locked by joints. Each turn is a slotted circular ring connected with the neighbouring rings near the slot (current cross-over). The coils are mounted on the vacuum vessel by supports (16 for each coil) movable to compensate distortions. The cross-over region and the current leadins of each coil are placed in one of the 16 sectors divided by the supports. The joints of all coils are situated in two other sectors.

The main material of the conductors is copper. In highly stressed regions we use beryllium-copper alloy. All leadins consist of three conductors in order to avoid forces resulting from the inhomogenity of the toroidal and poloidal magnetic fields. To permit easy manufacturing the conductors within the joints re-

gion are straightened and some of them are also cranked. All windings are insulated from each other with materials resistant to compression and high voltage.

The most important dates of the coils are:

a)	mean diameters:	MP 1	2710 mm
		MP 2	3033 mm
		MP 3	3454 mm
b)	number of turns:	MP 1	4 windings
		MP 2	8 windings
		MP 3	4 windings
c)	conductor cross-section:	1456 mm^2	
d)	electrical resistance of a triplet:	2,1 mΩ	
e)	inductivity of the coils:	0,5628 mH	
f)	current maximum:	45 kA	
g)	heating/pulse:	50^{o} C	
h)	stored inductive energy	570 kWs	

Loads

Normal operating conditions call for an opposite series connection of MP 1 and 3 with MP 2. The current polarity of MP 2 and the plasma are equal. The MPs are placed in the toroidal and poloidal magnetic fields and in the field of the plasma. The field of the OHs can be neglected.

During the current pulse the MPs are heated and stressed only by magnetic forces. The heating of the MPs does not effect distortions between the windings of a MP. The windings of each MP 1 and 3 and the upper and lower windings of MP 2 form part of a coolant loop. During cooling between the windings arise differences of temperature and distortions stressing the conductors and the insulation.

Within a normal sector there exist electro-magnetic forces in the radial (r) and vertical (z) directions but not in the toroidal (φ) direction (Fig. 3). The values of this forces are calculated by a computer program /2/ and they depend on the different operating conditions. Because the conductors in the joint region are straightened and cranked, additional forces are exerted. This also is real for the cross-over region. The forces stress the material in the cross-over or joint region and induce also bending moments in the adjacent sectors. Furthermore, forces arise caused by plasma motion.

The leads for stabilizing the plasma placed beside the MP 1 and MP 3 but not within the joints region yield assymmetric forces within the MPs.

The loads acting to the leadins are induced

1) by the currents in the leadins ($^{k}_{RE}$),
2) by the toroidal magnetic field ($^{k}_{RH}$), and
3) by the poloidal magnetic field ($^{k}_{\varphi pol}$).

Force $^{k}_{RE}$ is constant to the whole length of a leadin and the forces exactly cancel each other if the conductors are frictionally connected. The forces $^{k}_{RH}$ nearly cancel each other, because there is nearly linearity between the toroidal field and the radius R within the conductor region. Only forces $^{k}_{\varphi pol}$ do not cancel each other, but the resulting forces acting on the whole leadins are very small and the main point of action is in the vicinity of the coil, only giving uncritical bending moments.

Computation methods

To select a suitable method of computing distortion, load distribution and stress of the MP coils we used the following general criteria:

1) The computed results must be as realistic as possible.
2) Results of a computer have to be checked. Methods with no possibility of checking are unsuitable.
3) Easy reproduction of the results is necessary for computing several runs to obtain optimum results.
4) The expenditure for computing has to be acceptable.

If analytic computing methods are not practicable we made use of the finite element (FEM) method. FEM computer programs being applied to this problem are Strudl and Sap /3 a. 4/.

A perfect way yielding exact results would be to compute the coil as one unit. This is very expensive and the capacity of the available computer is not sufficient. Analytic considerations show the qualitative stress in the various coil-sectors. We thus found four types of sectors for which the stress has to be determined:

1) Undisturbed sectors: Because of the symmetric construction

and load in this sectors the stress has to be computed only in one half of the sector.

2) Sector with joints: This sector is also symmetrically constructed and loaded. Stress in one half must be computed.

3) Sector with current cross-over: The stress all over this sector must be computed.

4) Sectors adjacent to the cross-over and joints region: We have to decide between sectors

   a) near the cross-over region,
   b) near the joints region, and
   c) near the cross-over and joints region (this is only one sector in each coil).

   A special feature of a stress analysis is for coils is always the electrical insulation. In view of its indeterminate mechanical properties the insulation is the most critical material of a coil. We considered two fundamental ways of insulating the MP coils:

   1) The single conductors are completely insulated and the conductor pack is combined by a surrounding elastic insulation binding. The insulation between the conductors can only be stressed by pressure. Loads that fan out or displace the conductors toward each other stress only the conductors on the surrounding isolation. Tension and shear do <u>not</u> stress the insulation between the leads.

   2) There is also an insulation between the conductors, but the insulation as a whole forms a single connected structure. The insulation between the conductors and the interface are thus highly stressed by tension, pressure and shear. The conductor material will thus be less stressed.

   Insulation type 1 involves more expensive manufacturing than insulation type 2; but the reliability of coils of type 1 seems to be higher.

The FEM model chosen is composed of beams and trusses. The beams placed in the centre of the cross-section are connected in "joints" and the number of beams ensures a fairly realistic distortion of the conductor. The "joints" of adjacent leads are connected by trusses (Fig. 4,5,6) with extremely high stiffness. The calculated loads of the trusses give the stresses of the insulation between the leads. MP coils of type 1 may be calculated if all trusses with positive loads are eliminated. The insulation is thus only stressed by pressure. If we do not eliminate trusses stressed by tension we obtain approximate results for MP coils of

type 2. Shear stresses within the insulation due to displacement of the conductors to each other are not very realistic. Such values are too high. One has to use a model simulating the whole volume of the conductor and insulation.

Results of computation

If we compare the stresses in the joint region with the undisturbed region (Fig. 4) the effect of the additional forces and bending within the cranked and straightend region is demonstrated. Wedging the conductors in the contact region reduces the stresses within the joint region of about 50 %. The additional forces and bendings within the cross-over region cause five times higher stresses than within the normal sector. Furthermore, we computed remarkable displacements of the conductors within this region. Owing to this the insulation within the cross-over region is highly stressed. We found out that the surrounding insulation has to be thickened for 15 times to withstand the forces and bendings acting to it. The design of the MPs is based on the computed results and we could undertake doing following constructive details:

1) Cross-over and joint regions have to be constructed from CuBe alloy.
2) Cranked and straightened joints can be installed to manufacture and set up the coils in an easy way.
3) Wedging of the joints is advantageous.
4) Special bracing for the cranked parts of the leadins in the cross-over region is necessary.
5) The coolant loops are connected in such a way that during cooling the winding with a large diameter is colder than the adjacent winding with a smaller one.
6) To braze parts of the windings together minimum stressed positions were determined.
7) The bolts for mounting the joints must be manufactured from CuBe with high strength.

The computed results for the coils of type 2 are unsatisfactory. We therefore test a model at present which completely considers the insulation of a coil.

References

(1) Hartz F. et al.
technical concept for the multipole coil of ASDEX.
Proc. 9th Symp. on Fus.Techn. 1976, p. 197

(2) Martin, P.; Preis, H.
Program description and users manual for the Hedo 2 magnetic field computer program.
Report IPP III/34

(3) Othmer, O.
ICES-STRUDL Application Manual Vol. I and II
ICES-STRUCL Operation Manual.
Messerschmitt-Bölkow-Blohm, 1976

(4) Bathe K.J. et al.
SAP IV A Structural Analysis program.
University of Southern California, 1974

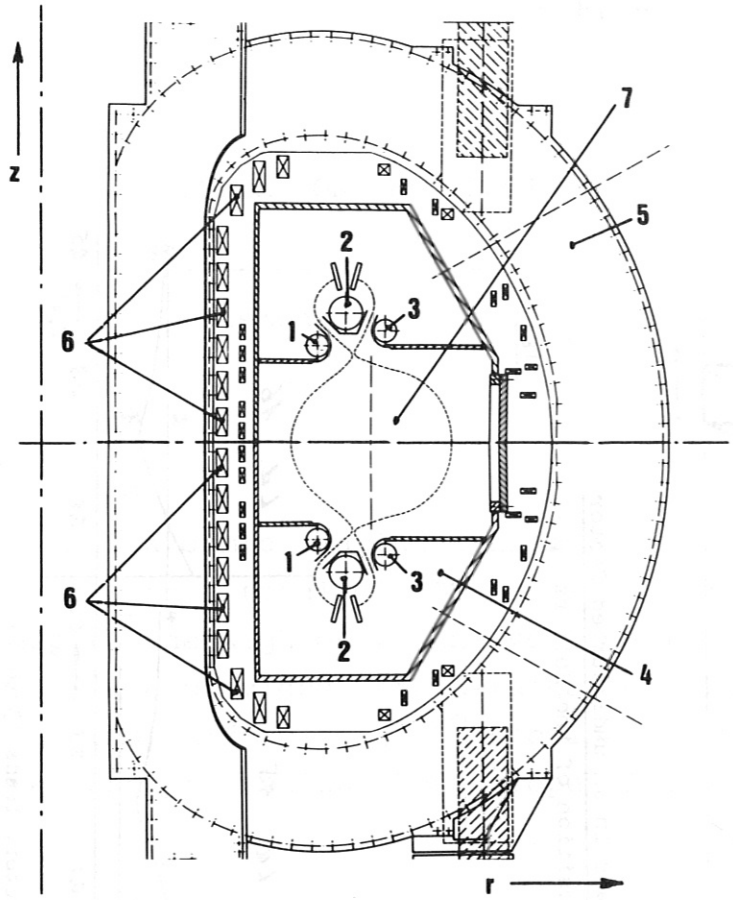

Sectional View of ASDEX

1 MP Coil 1; 2 MP Coil 2; 3 MP Coil 3;
4 Vacuum Vessel; 5 Torodial field coil;
6 OH Transformer coils; 7 Plasma;

Fig. 1

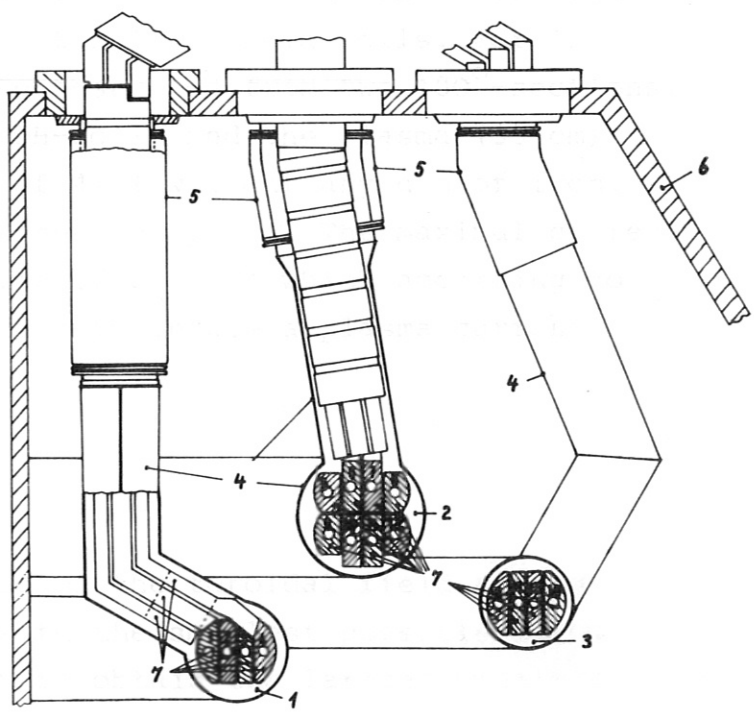

Leads-in and Cross-section of the MP-Coils

1 MP-Coil 1; 2 MP-Coil 2; 3 MP-Coil 3;
4 Shielding Tubes; 5 Bellows; 6 Vessel;
7 Conductors of the Coil;

Fig. 2

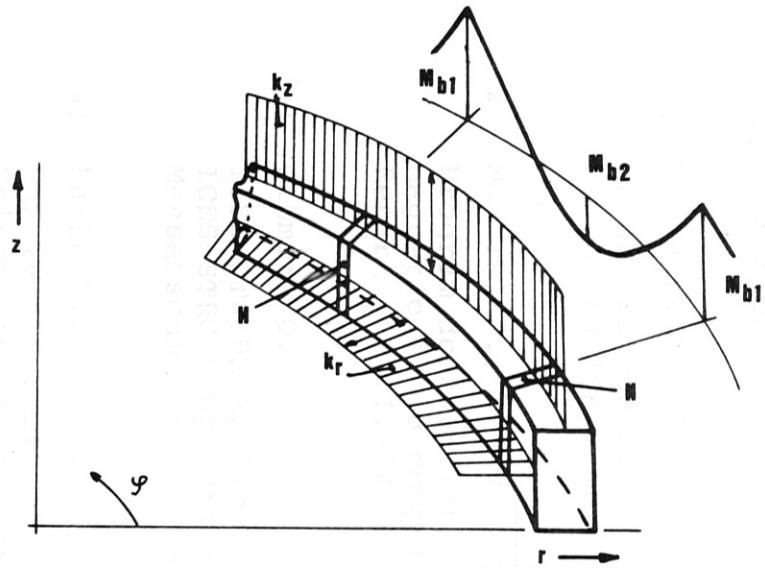

Loads in an undisturbed Sector
- Position of the Holders H -

Fig. 3

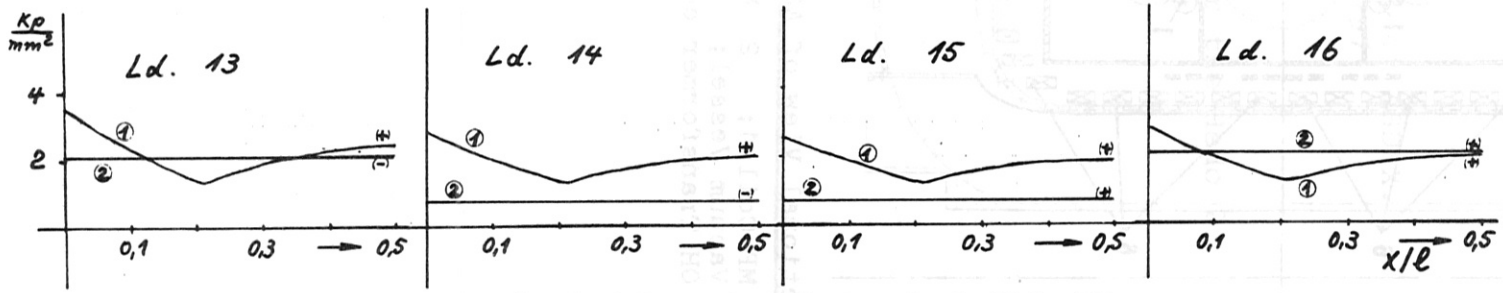

Stress of the MP 3 Normal Sector (graphed for each conductor; leads 13 to 16)
1) electro-magnetic stress; 2) thermal stress at cooling down; l = length of the sector;

Fig. 4

DESIGN, CALCULATION AND TESTING OF THE ASDEX OHMIC HEATING COILS

Klement,G., Preis,H., Wedler,H.

Abstract

The ASDEX ohmic heating transformer consists of 24 separate coils with a total of 100 turns with diameters up to 5 m. Despite the high operating voltage (20 kV) all of the OH coils are provided with detachable joints and can be divided into two half-coils (180^{o} sections) for installation purposes. The concept ensuing these properties is discussed in detail.

Introduction

ASDEX is a Tokamak which incorporates an axisymmetric divertor. Its purpose is to produce high temperature plasma (T_e: 4 keV) /1/. A cross-sectional view of the experiment is shown in Fig.1 (picture of a wooden model). In order to obtain a good coupling with the plasma all 24 OH-coils are placed between the vacuum vessel and the 16 toroidal field coils. For installation purposes they are assembled from two 180^{o}-sections. The short distance between OH-coils and the plasma (35 cm) results in a high coupling of 47 % without any use of iron. 3.8 MJ can be stored within the OH-system. The maximal current of 30 kA yields a flux swing of 2.54 Vs which according to current estimates will suffice to induce a plasma current of 500 kA /2/.

Technical Concept

Because of the r^{-1} variation of the toroidal field a very compact coil construction with the smallest possible torus radius is required in order to obtain the largest possible

useful volume with high magnetic flux density. Four separate coil systems with 3.2 MA windings and operating voltages up to 20 kV have to be accomodated within the small space between the vacuum vessel and the toroidal field coils (distance: 17 cm). The splitting up of the coils calls for joints which must take up the entire centrifugal forces and guarantee good electrical contact at an insulation level of 20 kV. These requirements have to be accomplished without allowing the joints to occupy more space than the coil cross-section itself. Their positioning inside the toroidal field coils acutally at the maximum of the toroidal field (60 kG) results in high forces (180 kp/cm), requiring complicated support structures, wherever there is a deviation from axial symmetry, such as at the coil leads and crossovers.

Figure 2 shows three OH-coils during test assembly prior to their installation into the experiment, which can be seen in the background. The two joint positions (a,b), each with 4 Berylco bands aside, connections for cooling water (C), and coil crossovers (d) are especially typical for this coil concept, as the coils are not spirally wound as usual.

Figure 3 was taken in July 77 during installation of the OH-coils. This is an exceedingly subtle process, as close fits at the contact positions are necessary. Therefore, each coil was premounted in order to align the coils to achieve optimal fitting at the contacts. The vertical forces (up to 32 tons/coil) are taken up by crossbars bolted to the 16 toroidal field coils with fitting bolts. To reduce the mechanical stresses, these crossbars are additionally supported against each other on the outside by means of vertical beams (f). The 9 inside coils on top exert a force of 120 tons against the 9 coils underneath. The crossbars only support the vertical forces. The coils are free to expand radially. When the OH current is switched on, the toroidal field coils are tilted in toroidal direction by 1 mm. When the current is

switched off in 30 ms, accelerations of up to 4 g arise. Since the OH-coils also take part in this motion, they are clamped together at 4 postions (e) by aluminium beams which are fitted toroidally into the toroidal field coils and are allowed to slide radially. The coil crossover is located at position e, too. The compensating conductor which is positioned 5 cm behind the crossover reduces the field distortion caused by the coil leads to $<$ 25 G in the region of the plasma. The forces of 180 kp/cm exerted on the crossovers due to interaction with the toroidal field are also taken up by the aluminium beams (e)

Construction and insulation of the coils

The coils, made at BBC in Mannheim in cooperation with the IPP, consist of 1 - 6 turns with a copper cross-section of 945 mm^2 (see Fig.4). A 1 mm layer of glass fibre insulation is wrapped around each turn. To allow for tolerances a 1 mm air gap has been provided and filled with insulating mats. The coil insulation consists of 5 mm thick glass fibre-mica tape. The coil halves are impregnated in vacuum and cured at 120° C /3/. Coil insulation characteristics are:

Operating voltage:	20 kV peak
Testvoltage:	40 kV peak, 50 Hz, 1 min
Inter-turn voltage:	200 V
Inter-turn voltage (test):	2 kV peak, 50 Hz, 1 min
Compression strength	20 kp/mm^2
Tensile strength	19 kp/mm^2
Shear strength between copper and insulation:	0.5 kp/mm^2

An important consideration for the insulation is protection against glow discharges. The end of a coil half is depicted on the right of Fig.4. The surface of the insulation in the undistorted region of the coil is covered with a conductivity layer (dashed area in Fig.4), which is connected at one point

to the experiment earth. For a distance of 11 cm from the coil ends a semiconducting layer is put on to ensure even voltage distribution (E = const. = 1.8 kV/cm). The insulation coating used for the joints is similarly protected against glow discharges.

Coil joint

A tension of up to 2 tons/turn , superimposed to the vertical forces of 23 kp/cm, arises at the joints as resultant of the centrifugal forces. From a series of proposals, a toothed joint was developed (Fig.5). Sixteen teeth make contact, so that, given an ideal fit and a symmetrical load distribution stresses of 12 kp/mm^2 arise at the troughs between the teeth. Four Berylco bands press the contact bridge with 600 kp/band into the coil ends. A slender tooth shape ($\sphericalangle$ 45°) was chosen so that manufacturing tolerances up to 20 µ could be compensated by deformation of the teeth. A symmetrical load distribution and a reduction of the bending stresses are achieved by tilting the set of teeth. A 10 µ thick silver coating provides further improvement. The total contact surface is 1520 mm^2, of this 610 mm^2 (50 A/mm^2) are pressed together by the centrifugal forces (3 kp/mm^2). To keep stress concentration effects as small as possible, a radius of .5mm was used between the teeth. For a tightening moment of .8 mkp, contact resistance was 3 µΩ/turn (i=1000 A) which centrifugal force reduced to 2 µΩ/turn (i=30 kA).

Coil test

Before production started the coil-test-joints were examined with a microscope at a magnification of 40 for gaps between the teeth. At .5 mkp three teeth showed gaps up to 20 µ,which disappeared except for one tooth with a 10 µ gap at .8 mkp. As a safety measure all the contacts are colour coated for test assembly. Figure 6 shows the contacts with the coating. The

thickness of the coating is about 5 µ which implies that at those contact surfaces which are not colour coated (20 %) the gap has to be at least $\geq$5 µ.

The contacts were also mechanically tested. A tension test was carried out with 500.000 cycles at 1.5 times the nominal load, after which the contacts were torn apart in a crash test at 5 times the nominal load (10 tons). A test contact was also electrically tested at 30 kA (1000 cycles). No welding spots have been observed.

The finished coils are tested at 40 kV peak, 50 Hz for 1 minute. The measurement of the coil resistance and $tg\delta = f(U)$ complete this test program. A water pressure test with 50 bars was carried out and the water flow was measured.

Field and force calculations

Figure 7 depicts the magnetic field lines of the described OH coil system. The field lines were calculated and plotted with the aid of the computer program HEDO 2 /5/ whose theoretical basis is presented in /6/. By the special arrangement of the OH coils it could be achieved that the field lines do not cross the plasma column.

To avoid disturbing the plasma discharge, the stray field due to the OH-current must not exceed 10 G in the plasma region. The simplest way to check this requirement is by means of a niveau line plot. Niveau lines are here lines on which the magnetic flux density $|B_{(R,\varphi\ Z)}| = B_h, h = 1(1)\ n$ takes a discrete value B_h /6/. Owing to the axial symmetry of the OH coil system it suffices to show the niveau lines in a meridional plane. The calculation and graphical representation of the niveau lines was performed by the above mentioned program HEDO 2 (Fig.8). It is clear from this plot, that the flux density is nowhere greater than 10 G, so the required condition is met.

It is also useful to calculate the stray field outside the experiment where diagnostic equipment sensitive to external fields is placed. This is best shown by a vector diagram, from which both field strength and field direction can be read (Fig.9).

Precise analysis of the forces acting on the individual turns under various operating conditions was required for the OH coils. This was carried out using the program HEDO 2. The resulting forces on each coil are shown in Fig.10.

References

/1/ The ASDEX Group:
Divertor Tokamak ASDEX, IPP III/27, July 1976

/2/ H.Preis,H.Wedler:
The ASDEX Ohmic Heating Electrical System,
Proc.of the 9th Symp. on Fusion Technology,
Garmisch-Partenkrichen 1976, p. 753 - 758

/3/ J.Scheel, H.Pauler:
Micadur-Compact-Isolation für rotierende Hochspannungs-maschinen mittlerer Leistung, BBC Nachrichte, Jahrg.53,H.1/2

/4/ L.Maduschka:
Beanspruchung von Schraubenverbindungen und zweckmäßige Gestaltung von Gewindeträger, Forschung auf dem Gebiet des Ingenieurwesens 7 (1936), S.299-305

/5/ P.Martin , H.Preis:
Program Description and Users' Manual for the HEDO 2 Magnetic Field Computer Program, IPP III/34 April 1977

/6/ H.Preis: Calculation of the Magnetic Field, Magnetic Forces and Behaviour of Large Coil Systems for Fusion Experiments, IPP III/24 April 1976

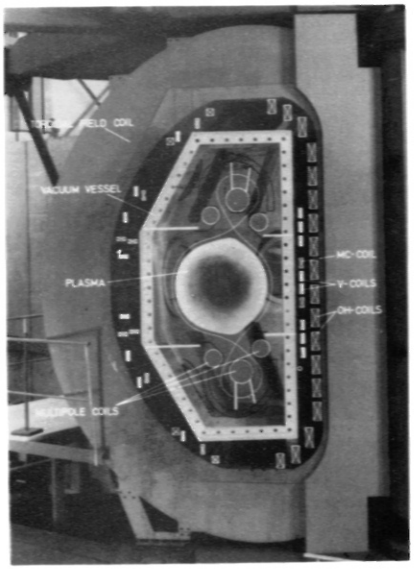

Fig.1: Model of ASDEX showing magnetic field coils and vacuum vessel

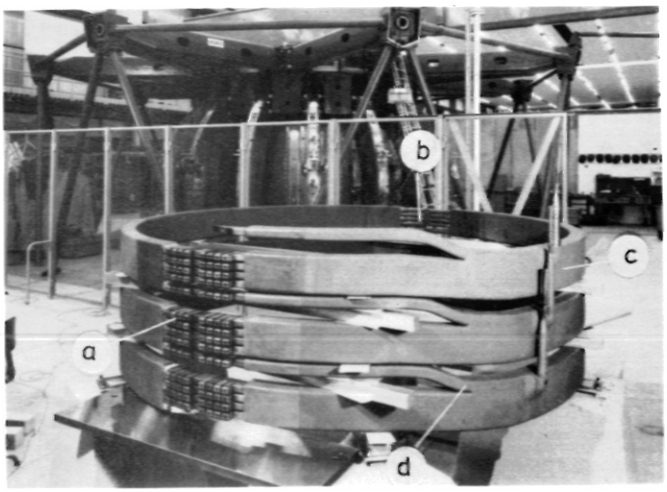

Fig.2: OH-coils during test installation

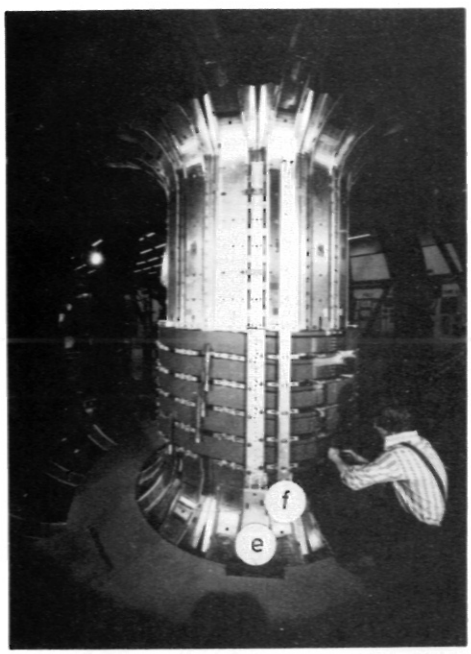

Fig.3: Installation of the OH-coils

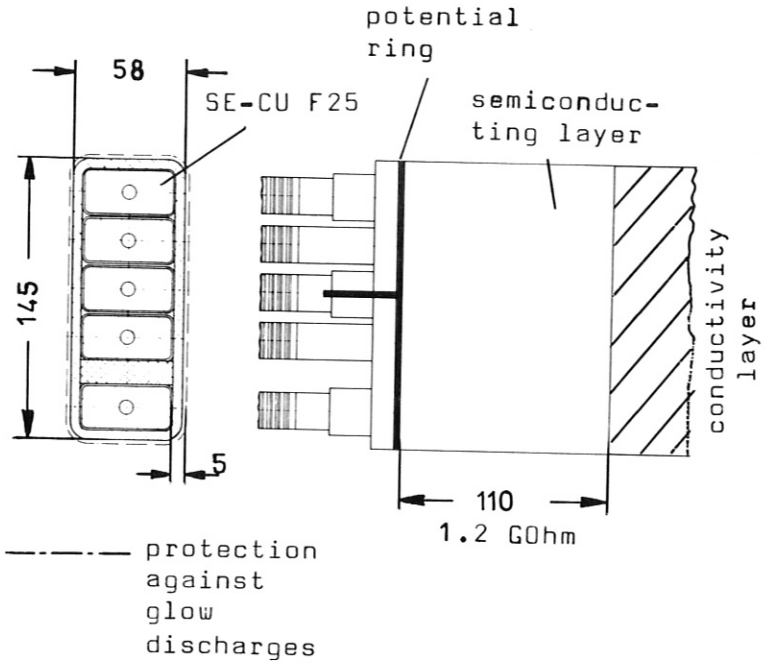

Fig.4: Coil construction and protection against glow discharges.

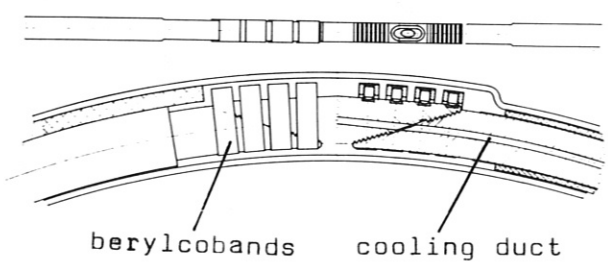

Fig.5: Toothed coil joint

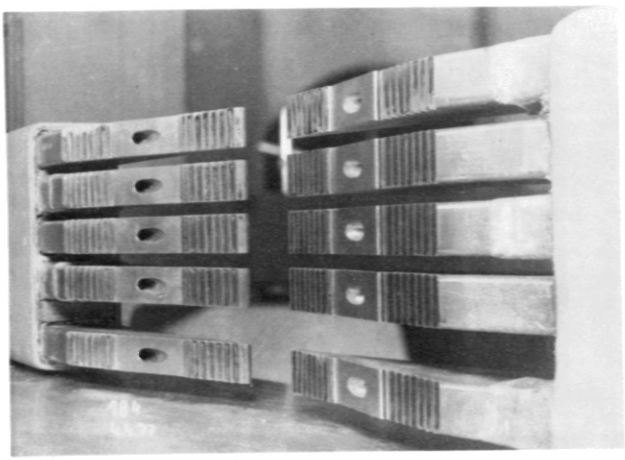

Fig.6: Demonstration of the fitting accuracy of the joints

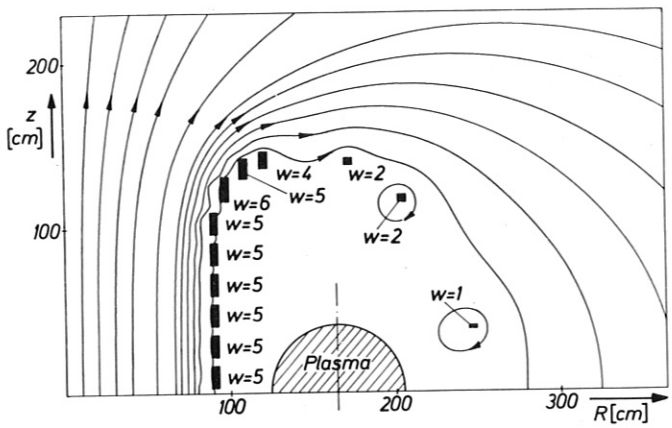

Fig.7: Magnetic field lines for the OH-transformer

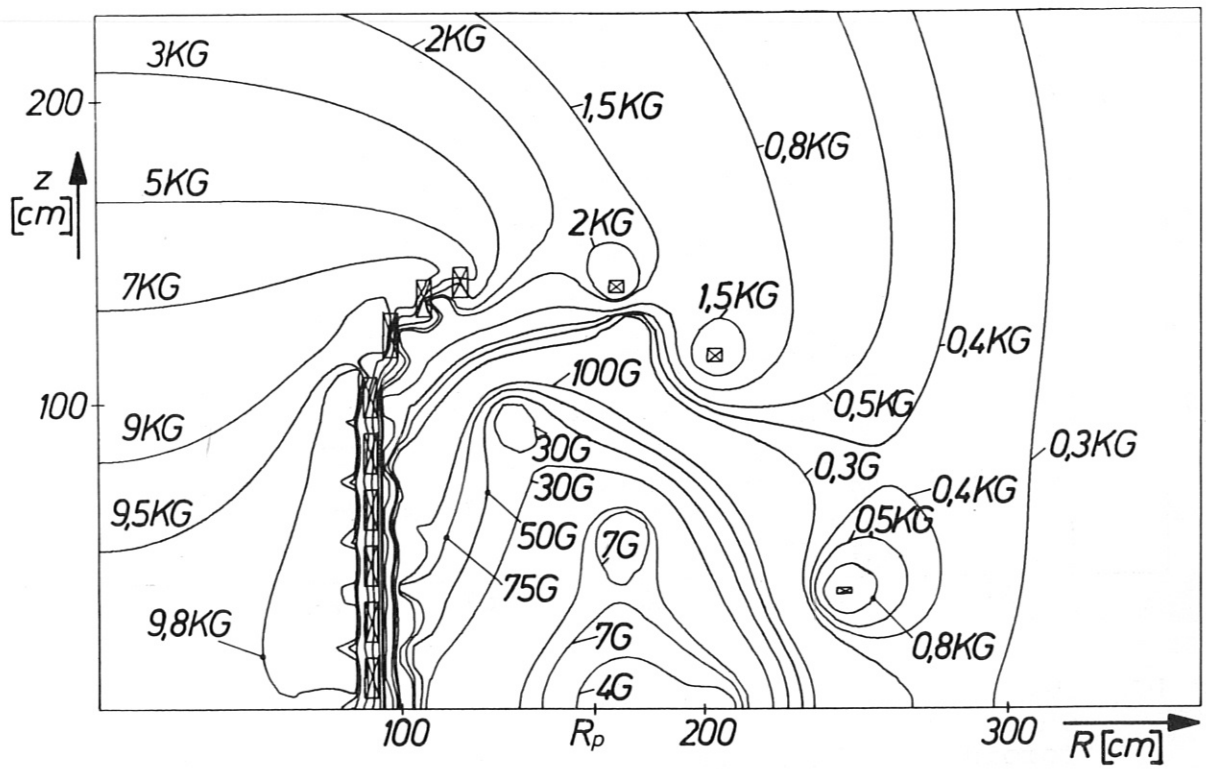

Fig.8: Magnetic niveau lines of the OH transformer

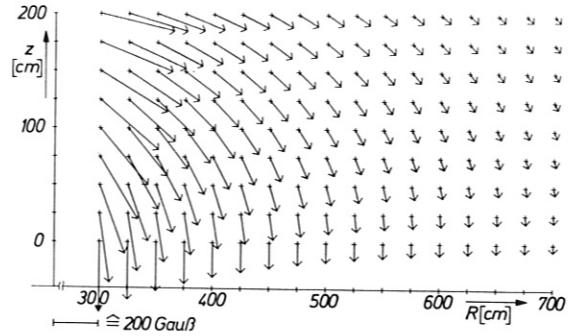

Fig.9: Vector diagram of the stray field outside the OH-system

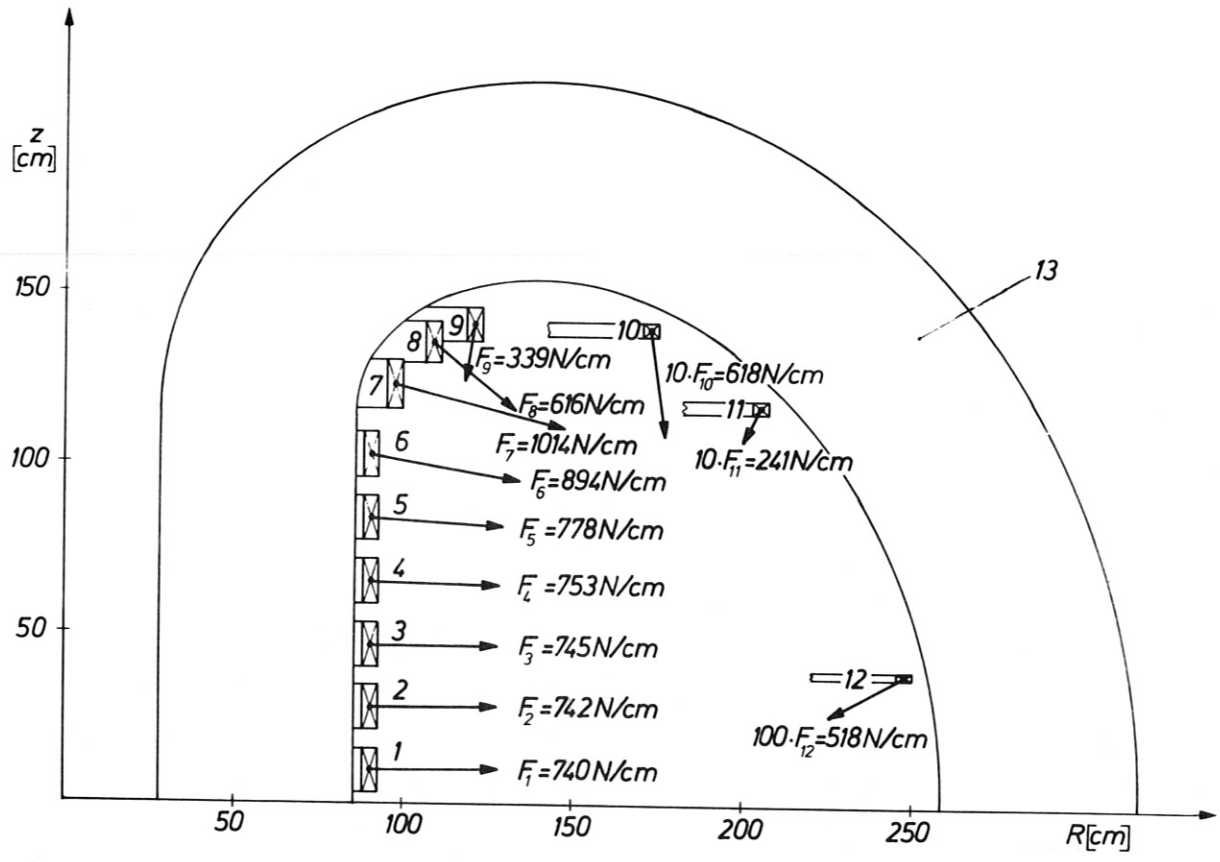

Fig.10: Magnetic forces per cm circumference of the OH-coils
OH-coils: 1 - 12
Toroidal field coil: 13

TESTING AND PERFORMANCE OF THE 30 KA OHMIC HEATING SYSTEM FOR ASDEX

Wedler,H., Gernhardt,J., Klement,G., v.Mark,E.

Abstract

After installation of the 18 inner coils for the ohmic heating system (90 of 100 turns) of ASDEX the coils were successively run up to the full current strength of 30 kA. At the same time the radial and vertical motions of the individual OH coils and leads were systematically investigated with 60 displacement pickups. In a further test phase the tilt motion of the toroidal coils at the full toroidal field (45 kA, 28 kG) was measured. The results of these investigations are discussed in detail and an account is given of experience with the breaker system.

Introduction

The objective of the ASDEX tokamak experiment with axisymmetric divertor has been reported /1/. The technical concept and the individual components of this machine have also been described in detail in several papers /2/. To give an insight into the problems involved in the OH-system, the aspects particularly critical for the OH coils /3/ are briefly presented. A detailed description is given in /4,5,6/.

In order to achieve good coupling with the plasma, the OH coils together with the vertical field coils, multipole compensation coils and radial field coils were accommodated in the very narrow space between the toroidal field coils and vacuum vessel (Fig.1). There is a maximum intervening space of 17 cm available to accommodate the stated four coil systems with their total of 3.2×10^6 ampere-turns and the necessary

current leads. A good impression of the spatial conditions is conveyed by Fig.2, which shows ASDEX with the ohmic heating coils completely installed. As the coils are located in the peak of the toroidal field, enormous forces of up to 180 kp/cm are exerted on conductor elements deviating from axial symmetry, i.e. coil cross-overs and leads. But owing to the toroidal field ripple axisymmetric conductor elements are also subjected to additional forces which cannot be neglected. Another special feature that should be mentioned is that for installation purposes the OH coils can be divided into two 180^{o} segments.

This affords the possibility of systematically testing the coil system together with the toroidal field but without the vacuum vessel and also monitoring it optically at the same time so that any weaknesses can be eliminated.

As a result of the centripetal forces (1000 to /coil) the TF housing moves 700 µ radially inwards in the symmetry plane (z = 0). On the other hand, the OH coils expand as a result of heating and the radial forces (350 µ). To keep the mechanical stresses in the copper as small as possible, the OH coils should be free to slide radially. To relieve the coil cross-overs, the coils are mechanically clamped together at four points on the circumference. The OH coils are prevented from rotating when the toroidal field coils tilt by wedging them in the toroidal direction with the main field coils by means of the four clamps. The vertical forces are taken up by aluminium strips attached to the TF housing.

Measuring and monitoring facilities

The water throughput in the individual cooling sections is measured with Venturi tubes. If the limiting value set is gone below, the system is switched off. The temerpature of

the outflowing water is recorded with temperature sensors and also monitored with limit indicators. As two cooling cycles at a time are operated together according to the diagram in Fig.3, reduction of the water throughput in a coil may lead to unacceptably high values of the coil temperature. The water temperature would not show any anomalous behaviour. To rule out any overheating of the coils, the temperature at the surface of the insulation of each coil is measured. As the penetration time of the heat wave into the coil insulation is longer than the cooling time of the coil (5 min), the temperature usually undergoes only a moderate rise ($\Delta\vartheta \sim 7^{\circ}$ C) at the coil surface for full temperature variation in copper ($\Delta\vartheta = 15^{\circ}$ C). Excess temperatures would, of course, quickly result at the coil surface if the cooling were to fail.

The motion was measured with linear potentiometers (Fig.4) of metal oxide. The signals were transmitted via different amplifiers to a 48-channel UV recorder or to storage oscilloscopes. The bandwidth of the complete system including the potentiometer is >3 kHz. All channels were calibrated prior to measurement. In general, the measuring accuracy was good and reproducible (rated value 600 μ, spread $\pm$ 70 μ). The positions of the individual pickups can be seen in Fig.5.

For the first time in the ASDEX coiltest we also used the 126-channel electronic limit monitoring unit consisting of the NEFF 620 and the PDP 11/20 limit monitoring facility. Exceeding the limits set leads to pulse interruption. In conjunction with the ASDEX computer it is possible to plot the signals recorded (PDP 11/70). The block circuit diagram of this monitoring facility is shown in Fig.6 /8/.

When the OH1 protoype coil was tested the nominal stress of coil was appreciably exceeded (factor 2.9) since the generator voltage regulator failed. As a result of this experience the

safety facilities were designed with great care. In the event of the current and voltage limits set (earth current and coil current) being exceeded the generator voltage is regulated down within 7 ms. To safeguard the coils in the event of regulator failure, the coils are short-circuited with the safety switch S3 within 10 ms.

General test after installation

On completion of the installation work the positions of the individual coils were determined at four different points around the circumference. All in all, the radial position tolerance of $< \pm 3$ mm is quite acceptable, as also is the axial displacement, which was measured to be $< \pm 3$ mm max., and which partly contributes to tilting of $< 0.2^{o}$.

The positional deviations were used in control calculations, which proved that the separatrix is not disturbed by these deviations. The width of the islands on the q=2 surface is less than 1 cm and thus quite tolerable /7/. In addition, all 180 contacts were colour coated and the contact teeth were checked for proper fitting. The contact surface showed no change relative to the trial installation and is at least > 60 % of the theoretical value. After connection of all cooling pipes the entire system was subjected to a pressure test with 60 bar. The flow-rates of each individual coil are measured and listed in Table I.

Table I: Flow rates of OH coils

	OH1	OH2	OH3	OH4	OH5	OH6	OH7	OH8	OH9
top(l/min)	11.1	10.7	10.5	11.7	11.9	10.6	10.0	10.2	10.8
bottom(l/min)	11.5	10.1	10.1	10.6	11.0	11.0	10.8	9.7	10.6

water temperature: 21..22^{o} C
input pressure 15 bar
output pressure: 3.2 bar
flow velocity: $\sim$4.5 m/s

In a cycle of 13 pulses in 68 min with 6 kA/60 s it was found that the water temperature at the end of the series had only risen insignificantly ($\Delta\vartheta = 0.5^{\circ}$ C).

After the flow measurement the insulation resistance of the conductor insulation and coil insulation were measured. The values for the insulation between conductors (s = 3 mm, q = 26 dm^2) are $\geq$ 3 GΩ in all cases. For the coil insulation (s = 6 mm, q = 88 dm^2) the values also exceed $\geq$ 3 GΩ. The only exception was a half-coil which exhibited significantly low for the conductor insulation ($\sim$160 kΩ) when tested. By heating to 90° C (24 h) it was possible to raise the resistance value to $\geq$ 13 MΩ. The ends of all half-coils, through which moisture presumably entered the coil, were resealed. Finally, the individual turns were tested against one another with a peak voltage of 2 kV, 50 Hz, 1 min, and the coil insulation with a peak of 20 kV, 50 Hz, 1 min.

Thermal cycles

The heating and cooling of the OH coils was controlled with temperature sensors on the coil insulation and at the cooling water outlets at current pulses corresponding to those to be involved later in ASDEX operation. The radial expansion induced by heating of the coils was measured at four locations on the circumference (Fig.5). Testing was done with the following current pulses: 10 kA to 40 s: $\int i^2dt$ = 3060 kA^2s/15 kA to 20 s: $\int i^2dt$ = 4500 kA^2s nominal ASDEX operation: 30 kA, 3s: $\int i^2dt$ = 2700 kA^2s.

In this phase a total of 100 pulses were shot. With 15 kA/20 s the copper is heated by 20° C. Even with these decidedly slow motions (cooling time 5 min) the displacement pickup signals are uniform and continuous. Furthermore, the motions are reversible, i.e. the zero positions of the pickups were constant over a cycle of 80 pulses. The motions are also easily reproducible.

The evaluation of a 10 kA/40 s pulse is shown in Table II. The following radial expansion is calculated for a 10 kA/40 s pulse: OH1-OH6: R = 905 mm, ΔR = 290 µ.

Table II: Radial expansion of OH coils

	bottom(µ)				top(µ)			
	TF3	TF6	TF11	TF14	TF3	TF6	TF11	TF14
OH1	150	250	50	300	100	150	200	300
OH2	100	300	0	400	100	150	300	350
OH3	100	450	0	500	300	200	350	400

As was also observed in the following tests, the bottom coil system, which is completely decoupled mechanically from the top one, does not slide at one location on the circumference (TF11). This disturbance is assessed later.

Consolidation of the OH coils

The current strength was successively increased up to the nominal current in stages of 100 pulses each to consolidate the coils, permanent set effects being checked at the same time. When the contacts were checked at the end of the test series the tightening torque of 92 of the total of 1440 screws had been reduced from 0.8 to 0.7 mkp, in one case to 0.6 mkp. All hard-tissue supports are gauged. No noticeable permanent set effects were observed.

Operation of OH coils with current interruption

With the installation of the inner OH coils the OH circuit required for the coil test was completed at the same time (Fig.7), but for the time being with a provisional water discharge resistance and a series-produced compressed-air breaker (AEG railway breaker). It was already demonstrated in 1977 that this breaker is suitable for the operating parameters aimed at /6/, but with a relatively short electrode lifetime of approx. 150 shots. Figure 8 shows the variation of the ring voltage at the plasma site. The negative spike before the vol-

tage rise that is produced by the commutation bank and the saturable inductor can largely be avoided by using, as planned, a heavy-duty breaker. The voltage rise can also be modified.

Joint operation of TF and OH coils with OH current interruption

In the final phase of the OH coil tests the OH coils were successively run up jointly with the TF coils. All particularly critical locations, such as coil cross-overs and leads, are optically observed with the theodolite and additionally with displacement pickups which were relocated from shot to shot. The timing of TF pulses (45 kA) and OH current pulses (30 kA) is shown in Fig.9.

The displacement pickup signals at the various OH coils and TF coils give the radial relative motion between the TF coil housing and the OH coil (Fig.10).

The TF current is switched on at time t_1. The centripetal force causes the TF coil housing to move inwards, the motion being greatest in the symmetry plane for z = 0 $\hat{=}$ OH1 (700 µ). Furthest out (OH9) there is hardly any radial motion present (200 µ). The amplitudes of these motions are listed in Table III. At time t_2 the TF coils are charged with 45 kA. The OH current starts at a time t_3. The amplitude of the radially outward motion of the OH coil is given in the right-hand column of the table (OH). The radial motion caused by the radial forces is much smaller. The thermal component is completely absent (30 kA, 3 s → 220 µ) since one has in this case $\int i^2 dt = 180\ kA^2 s$. A value of 130 µ is calculated for coils OH1-OH6 in consequence of the mechanical forces. Once the full OH operating current of 30 kA is reached the OH current is very quickly interrupted in 20 ms at time t_4.

Evaluation of this test series clearly demonstrate that the bottom OH coils do not slide at the coil TF11, i.e. the OH coils are taken along radially inwards by the TF coils at this point and deformed. The same effect is observed in the

top coil system at the coil TF14, but not so pronounced. In this case the sliding is as expected up to 300 µ, and then the OH coils are also bent inwards for the remaining 400 µ. In view of this disturbance all coils were checked in turn at 8 locations on the circumference. It was found that all observations are in agreement with the results discussed so far.

Table III: Radial movement between OH coils and TF coil casings (TF=45 kA; OH=30 kA).

		OH1(u)		OH3		OH5		OH7		OH9	
		TF	OH	TF	OH	TF	OH	TF	OH	TF	OH
bottom	TF3	675	175	610	125	475	100	275	125	50	0
	TF6	850	75	750	100	550	50	300	75	100	50
	TF11	50	100	60	100	70	50	100	250	50	0
	TF14	450	50	700	75	450	50	250	0	125	0
top	TF3	700	150	650	150	580	150	350	50	250	75
	TF6	580	80	430	0	380	0	100	180	150	0
	TF11	680	100	550	100	350	100	100	100	0	100
	TF14	350	0	375	0	300	0	250	0	50	100

The fact that the bottom coils do not in fact slide radially at coil T11 is somehow plausible and explicable since the electrical leads with clamps are located here. Calculations with SAP have shown that a 5-turn OH coil acted on by a force of 2300 kp is bent .7 mm inwards at one point. This stress is still tolerable. These investigations involved a total of 1650 shots.

References

/1/ M.Keilhacker: "Physics of Divertors and the Scrape-off-Layer", Report IPP III/42 (1978)

/2/ R.Allgeyer et al.; "The Design of the ASDEX Tokamak" Reprinted from 6th Symp.on Engineering Problems of Fusion Research

/3/ The coils were manufactured by BBC

/4/ H.Preis, H.Wedler: "The ASDEX Ohmic Heating Electrical System", Proc. of the 9th Symp. on Fusion Technology, Garmisch-Partenkirchen, 1976

/5/ G.Klement, H.Preis, H.Wedler: "Design, Calculation and Testing of the ASDEX Ohmic Heating Coils", Proc.6th Int.Conf.on Magnet Technology, Bratislava 1977

/6/ M.v.Mark, H.Preis, H.Wedler: "Design, Calculation and Testing of the ASDEX Circuit Breaker System", will be published

/7/ W.Feneberg: private communication

/8/ N.Ruhs: private communication

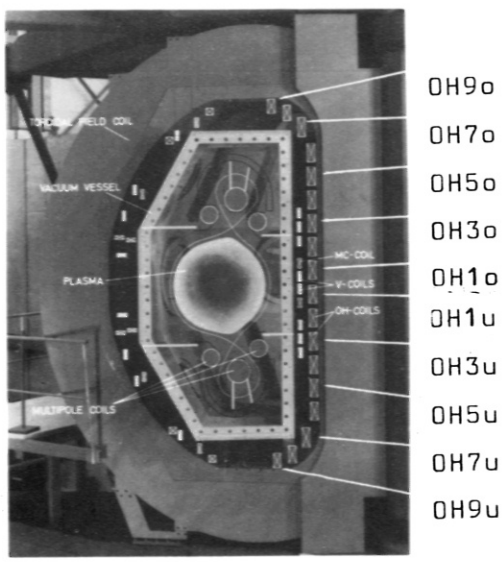

Fig.1:
Model of ASDEX showing magnetic field coils, vacuum vessel and position of displacement pick-ups for ohmic heating coils.

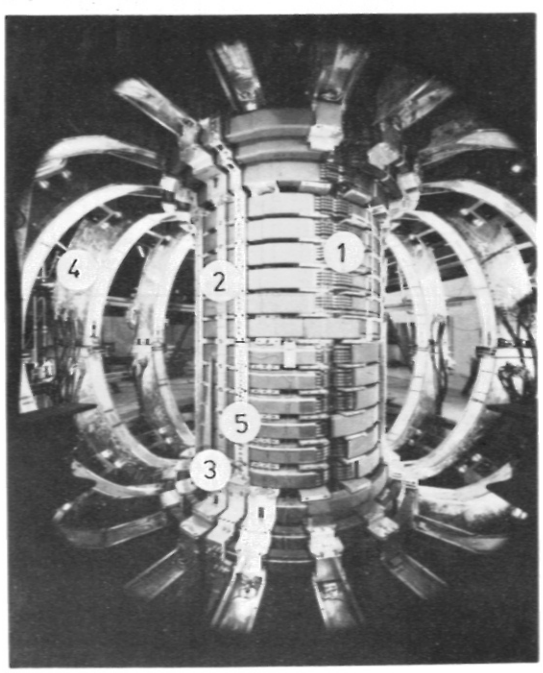

Fig.2:
Toroidal field coils (TF) and ohmic heating coils during installation
1. Demountable current connection
2. Alu-strips for taking up the vertical forces
3. Pipes for cooling water
4. Toroidal field cases
5. Clamps for fixing the coils

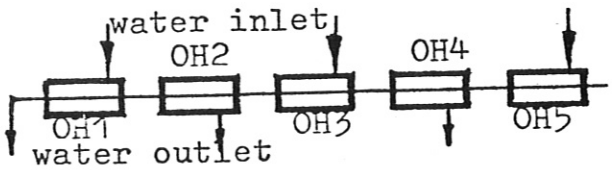

Fig.3:
Schematic representation of the OH-cooling system

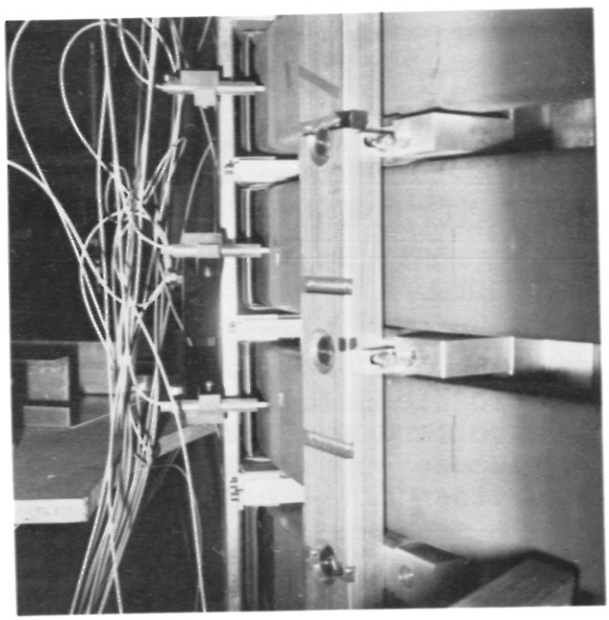

Fig.4:
Displacement pick-ups for measuring the relativ radial movement between toroidal coil housings and ohmic heating coils.

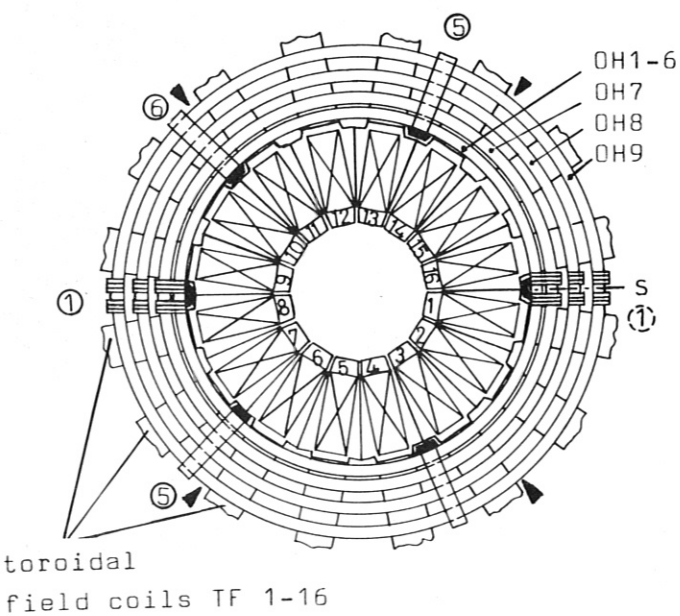

Fig.5:
Toroidal position of the displacement pick-ups( ) with demountable connections (1), coil cross-over (6) and clamps (5)

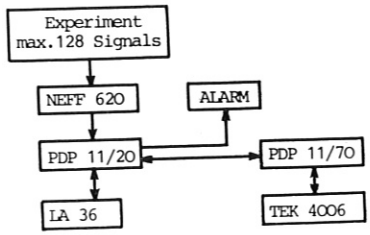

Fig.6: Block diagram of the monitoring unit

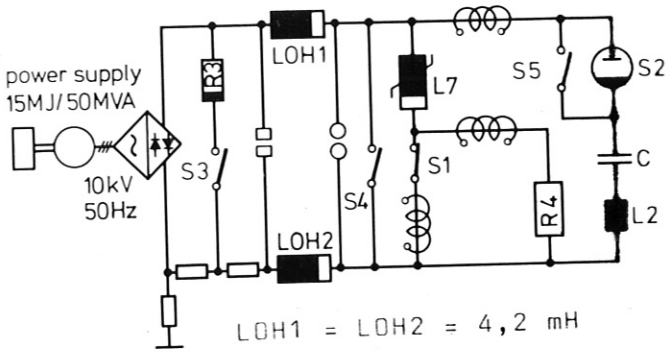

Fig.7: Circuit diagram of the ASDEX OH-system

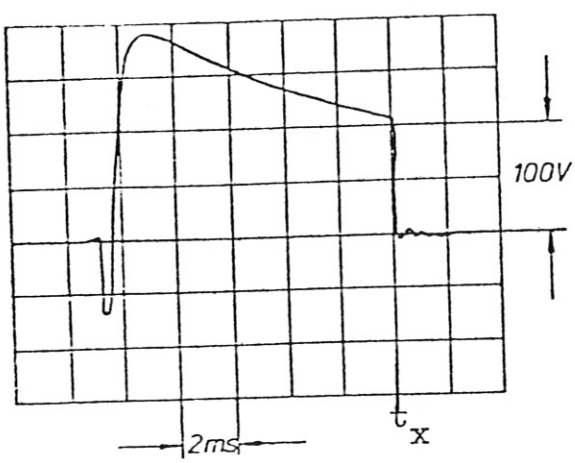

Fig.8: Measured ring voltage during ASDEX coil test with 30 kA. At t_x the switch S4 was closed

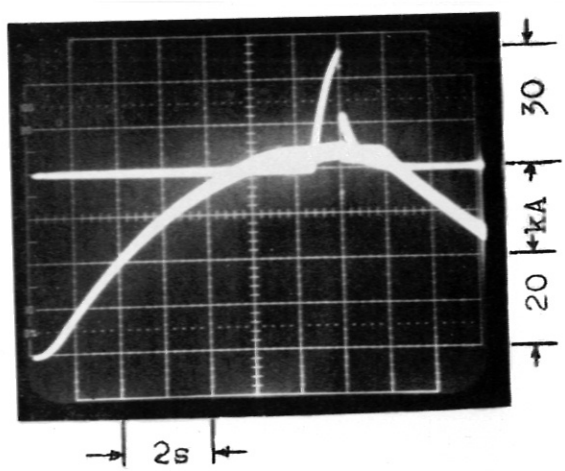

Fig.9: Toroidal coil (bottom) and OH-coil current

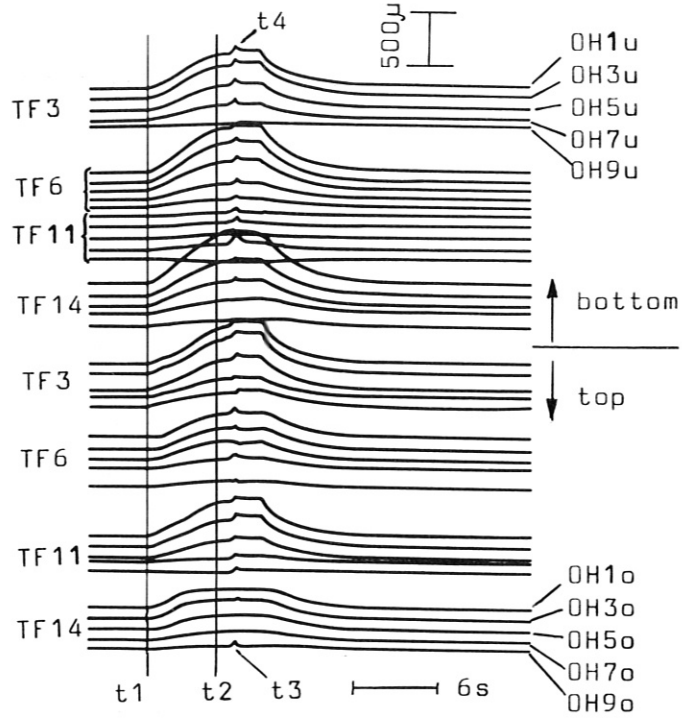

Fig.10: Radial movement between OH-coils and TF coil casings (TF=45 kA, OH=30 kA).

NOVEL METHOD OF DETERMINING THE PLASMA POSITION AND ITS APPLICATION TO THE ASDEX FEEDBACK SYSTEM

F. Schneider

Abstract:

In the ASDEX tokamak the plasma position will be directly determined by a combination of measurements of magnetic fluxes, fields and field gradients, not requiring knowledge of internal plasma parameters. The feedback system thus needs neither corrections for variation in the poloidal ß and the plasma current distribution nor compensation for the induced currents in the vacuum vessel.

It will be possible to set the plasma position with a simple potentiometer or with the computer by means of a special CAMAC module if a time dependent program is wanted.

Problem

The plasma position in tokamaks is usually determined with magnetic probes /1,2,3,4/. In existing facilities, however, the test signals depend not only on the plasma position (R) but also on the energy density (through $ß_p$) and the internal inductance (l_i) of the plasma.

(Note: These parameters are not needed by the measurement principle used in CLEO-Tokamak /2/, but there the centre of the plasma current is controlled, while the plasma boundary, in which we are more interested, is still affected by $ß_p$ and l_i).

It also matters whether a copper shell is used and what properties the vacuum vessel has. Many theories /5,6/, most of them making idealized assumptions, have been formulated to determine the equilibrium conditions and the various parameters.

In practice, difficulties are encountered in measuring the internal plasma parameters and including them quickly enough in calculation to regulate the plasma position. It is even more difficult to take the time dependent inductive currents in the vessel into account. Mathematical formulae are only available for tokamaks with circular poloidal cross-sections /6/.

It has not been possible to apply these theories to ASDEX with its multipoles and complicated vacuum vessel (see Fig.4 or 8). We therefore made measurements in a model on the scale 1:10 to investigate the induction currents and the reaction of the plasma to them /7/. In addition, the values were refined by making exact calculations /8/. The elaborate calculations are, of course, not suitable for immediate, continuous determination of the plasma position and its regulation during operation.

To obviate all these difficulties, we looked for a new measuring method capable of taking into account all influences, thus dispensing with the need for mathematical correction.

Treatment

The plasma boundary is always a flux surface. This is valid irrespective of what pressure prevails in the plasma and what current distribution is established or what induction currents act on the plasma. So if it were possible to install two flux measuring loops in close proximity to the plasma surface and to ensure with an ideal feedback control system that the flux in the two loops is always equal, this flux surface, i.e. the plasma boundary,would not change position, even if internal plasma parameters or the currents in the vessel were to vary.

This is the basic principle underlying the ASDEX feedback system with the position measuring method described here.

Solution

To determine the flux at the plasma surface, we do not necessarily have to make measurements there. It is sufficient to determine the flux at some distance if at the same time we also obtain the mean field strength (B_m) between the measuring loop and the plasma surface, multiply it by the intervening area (F_{px}), and add the result to the flux Ψ_x.

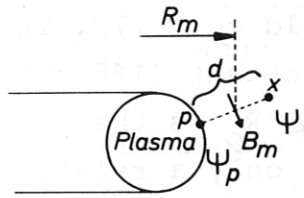

$$\Psi_p = \Psi_x + \int_x^p \vec{B} \cdot \vec{df}$$

$$\Psi_p = \Psi_x + \vec{B}_m \cdot \vec{F}_{px}$$

$$F_{px} = 2\pi \cdot R_m \cdot d$$

Nor must the mean field strength be measured exactly between the flux measuring loop and the plasma boundary if the field gradient ($\frac{dB}{dx}$) is known. In ASDEX it is determined by another coil.

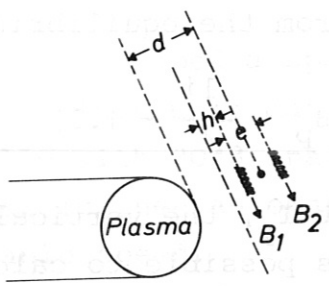

$$\frac{dB}{dx} \approx \frac{B_1 - B_2}{e}$$

$$B_m = B_1 + \frac{h}{e} \cdot (B_1 - B_2)$$

$$h = \frac{d - e}{2}$$

The sketch in Fig.3 is intended to illustrate the complete measuring and control principle.

The distance d_a and d_i between the measuring loop and a flux surface at the plasma boundary can be chosen arbitrarily and thus the position of the plasma can also be controlled. The diagram in Fig. 10 shows the electronic circuit. The reference input ΔR_{ref} controls the multiplying amplifier for avaluating the field strength signals. Combined with the signal of the flux measuring loops one obtains a difference flux signal, which can be regulated to zero by means of a regulator, thrystor amplifier and vertical field coil /7/. The plasma position is $R_p = R_o + R_p$ where R_o is constant (168 cm), ΔR_{ref} is the particular value required and ΔR_p is the deviation which in a good feedback system is just only a relatively small correction. It can be obtained from the quotient of the difference flux ($\Delta \Psi = \int \Delta \dot{\Psi} dt$) and the plasma current (J_p) without internal plasma parameters having any noticeable effect. Calculations of the resulting flux $\Delta \Psi$ in the measuring facility designed showed very good linearity with the plasma position R_p (Fig. 9).

Conversely, we have even devised a method of determining the internal plasma parameters from the equilibrium formula:

$$H_\perp = \frac{I_p}{4\pi R_p} \left(\ln \frac{8Rp}{a} + \beta_p + \frac{1i}{2} - 1.5 \right) \qquad /6/$$

As we know the plasma current I_p, the vertical field H and the plasma position R_p, it is possible to calculate $\beta_p + \frac{1i}{2}$.

For design reasons (owing to the multipoles and the diagnostic ports) the flux measuring loops were not mounted on the axis, but in the corners of the vessel. The positions of the measuring porbes can be seen in Fig. 4.

Owing to the high voltages at the vessel gap the flux measuring loops had to be interrrupted there (Fig. 5). Since, however, transient flux variations penetrate only through the gap, it was not possible to dispense with flux measurement at this location. We therefore installed a supplementary saddle coil over the gap outside the vessel (Fig. 6).

The photo (Fig.8) shows the interior of the original vacuum vessel with the flux measuring loops, but without multipoles and divertor cover plates (June 1978).

Calculations of the resulting flux $\Delta\Psi$ in the measuring facility designed showed very good linearity with the radial plasma position R_p (Fig.9).

Comparison between the magnitude to be measured and the exact position of the plasma showed only fractions of a centimetre difference over the whole range.

The radial position measurement for vertical field feedback as described is independent of the vertical position. In another combination however, the same probes will be used for vertical position measurement and radial field feedback. Good signals can be expected within 10 cm of the middle plane.

In ASDEX it will be possible to control the plasma position from the computer. In addition, the vertical field will also be programmed to achieve optimum control /7/.

For this purpose we developed a special control unit in CAMAC norm (Fig.11). This unit can be loaded from the computer or manually with 2048 analog values of 12 bits. On a trigger signal it then automatically issues this control curve with selectable speed.

The unit can also record voltage variations (transient recorder mode) and pass them to the computer. We thus cover various voltage variations, e.g. $\Delta\Psi$, R_p, I_p and I_v, in order to optimize by computer the vertical field control curve for the next shot.

The photo (Fig.12) shows the control panel for the plasma position, including the data acquisition and control units, and also the feedback electronics and process control computer.

Acknowledgement:

The author wishes to thank K.Lackner for suggesting the measuring principle and contributing to various discussions.

References:

/1/ L.A.Artsimovich: "Tokamak Devices", Nuclear Fusion 12 (1972) p.226

/2/ J.Hugill, A.Gibson: "Servo-control of plasma position in CLEO-tokamak", Nuclear Fusion 14 (1974) p.611

/3/ J.L.Anderson et al.: "Feedback control for plasma equilibrium in ORMAK" Nuclear Fusion 16 (1976) p. 629

/4/ R.Dei-Cas et al.: "Slow and fast feedback circuits for the plasma equilibrium in the TFR 600 Tokamak", Rapport EUR-CEA-FC 916 (1977)

/5/ J.M.Greene: "Tokamak equilibrium", Physics of Fluids 14 (1977) p.671

/6/ V.S.Mukhovatov, V.D.Schafranov: "Plasma equilibrium in a tokamak", Nuclear Fusion 11 (1971) p. 605

/7/ F.Schneider, F.Gresser: "Investigations on the feedback system of ASDEX", 9. SOFT 1976, Proc. p. 783

/8/ H.Preis: "Calculations of induced voltages and currents in the vacuum vessel of ASDEX" 10. Soft, Proc. , 1978

$$\Psi_{pa} = \Psi_a + \int_a^{pa} B \cdot df \approx \Psi_a + \underbrace{(B_{1a} + \frac{h_a}{e}(B_{1a} - B_{2a}))}_{B_{ma}} \cdot 2\pi \cdot R_{ma} \cdot d_a$$

$$\Psi_{pi} = \Psi_i + \int_i^{pi} B \cdot df \approx \Psi_i + (B_{1i} + \frac{h_i}{e}(B_{1i} - B_{2i})) \cdot 2\pi \cdot R_{mi} \cdot d_i$$

equal by Feedback

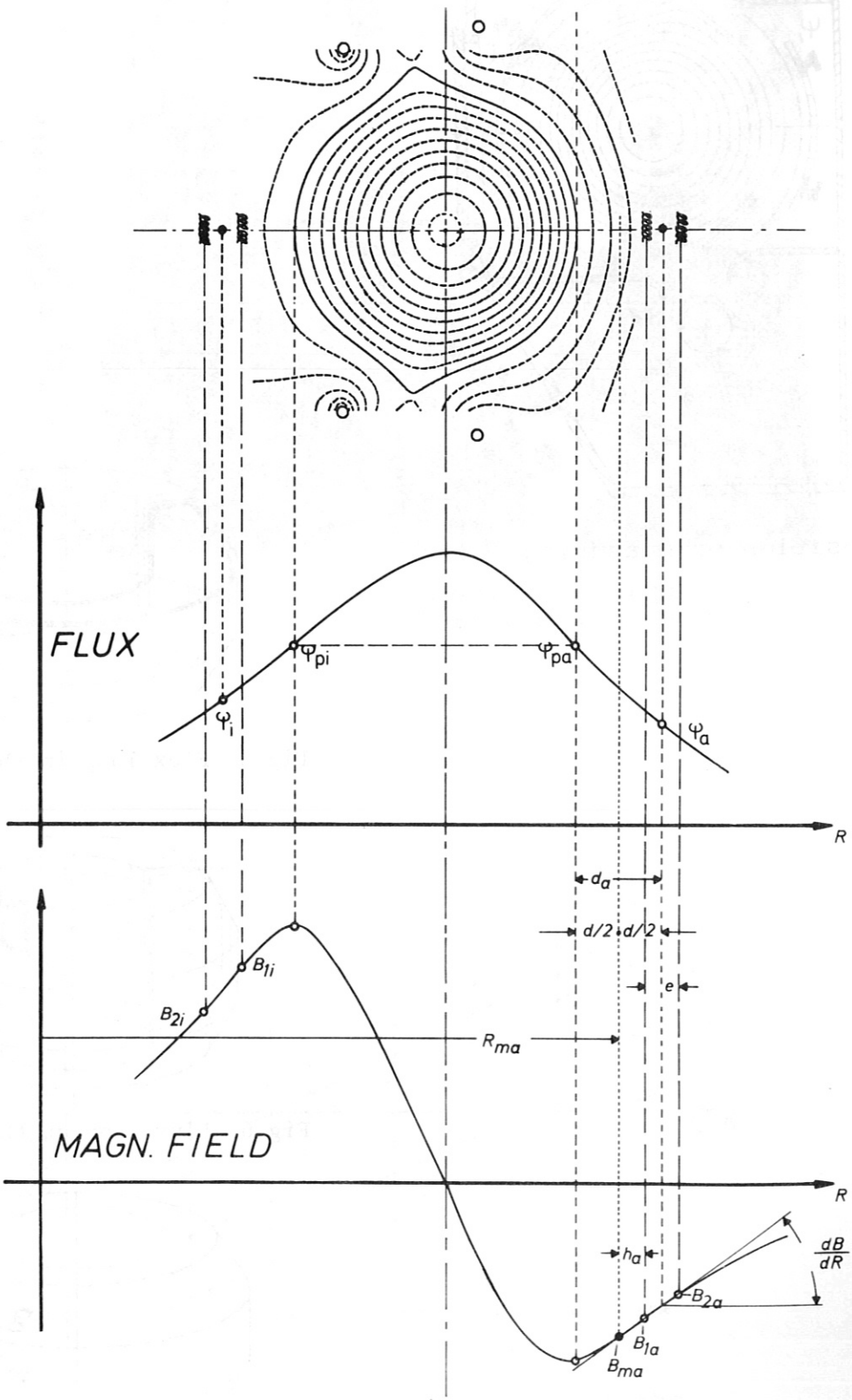

Fig.3: Illustration of the Mathematical Formulation of the Measuring Principle

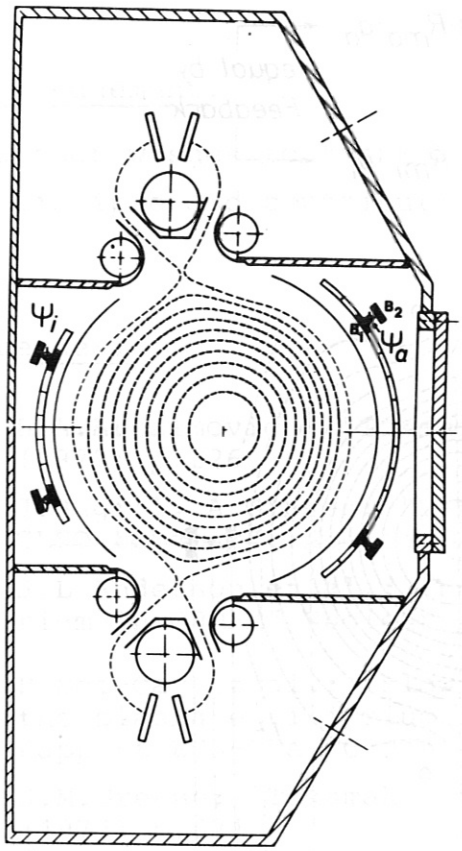

Fig. 4 Position of measuring coils

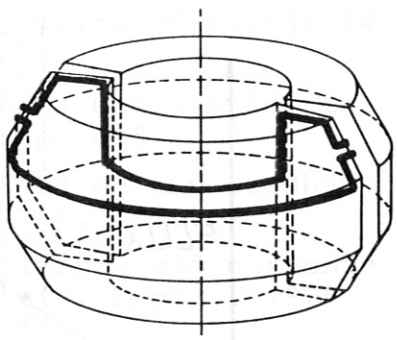

Fig.5 Flux loop in the vessel

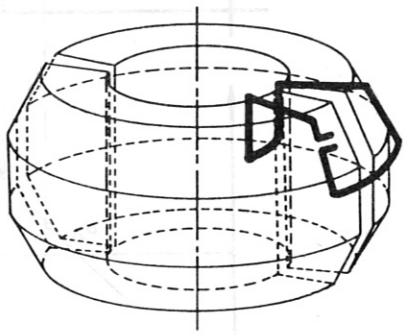

Fig.6 Flux loop at the gap

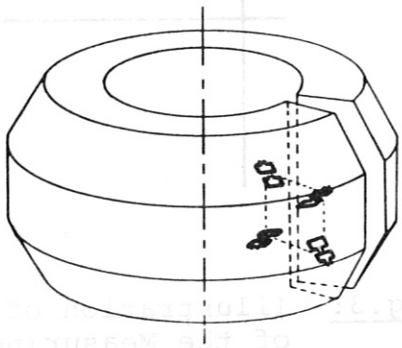

Fig.7 Magn.field coils in vessel

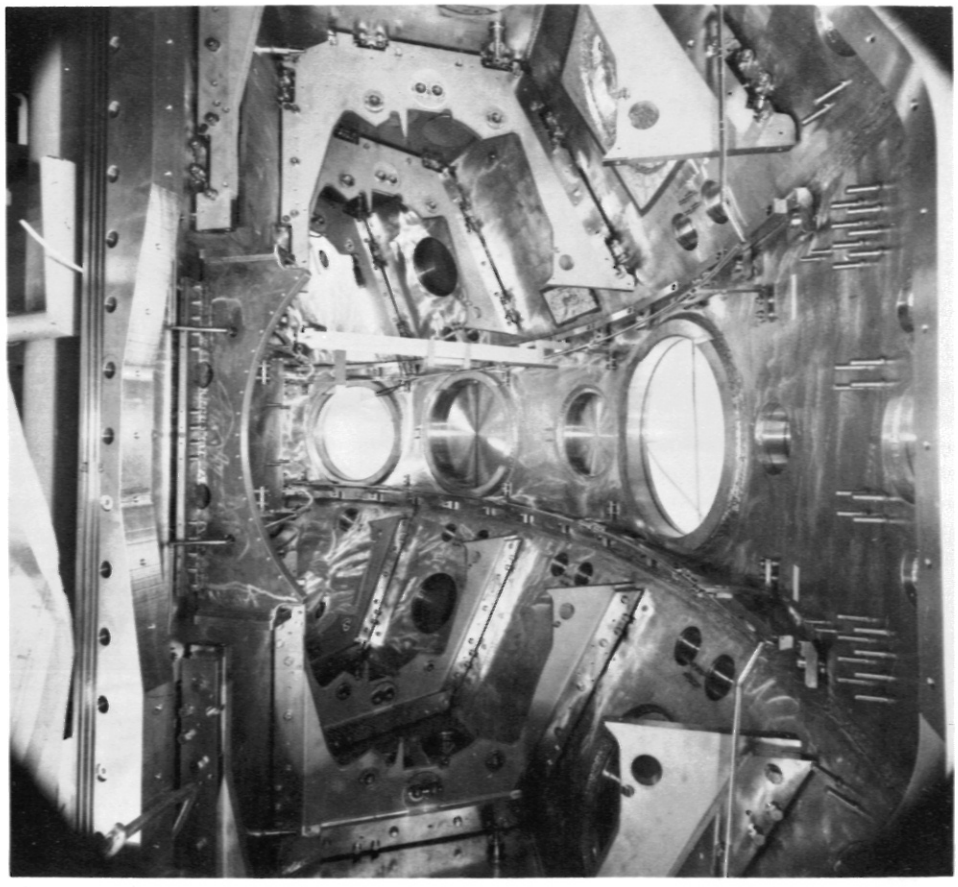

Fig.8 View of magn. Flux loops in the ASDEX vacuum vessel

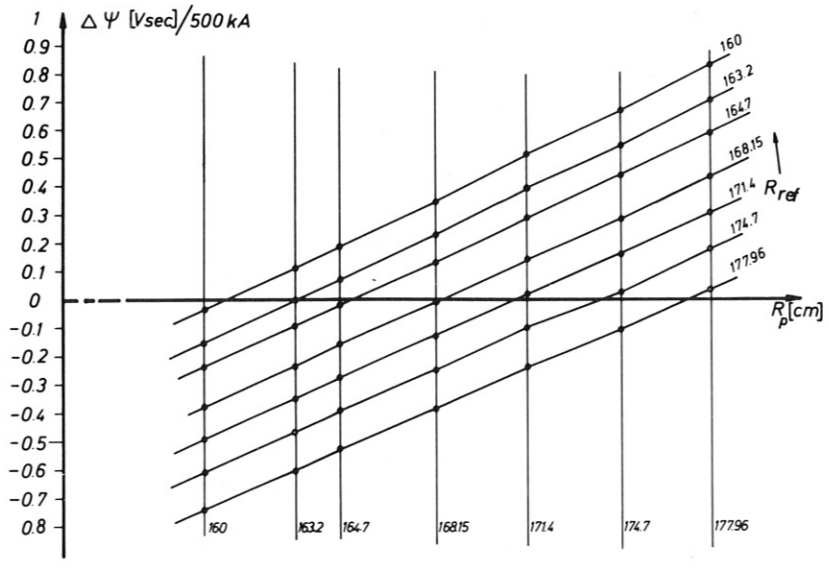

Fig.9: Calculated differential flux of the complete measuring system depending on the plasma position, with reference position as parameter

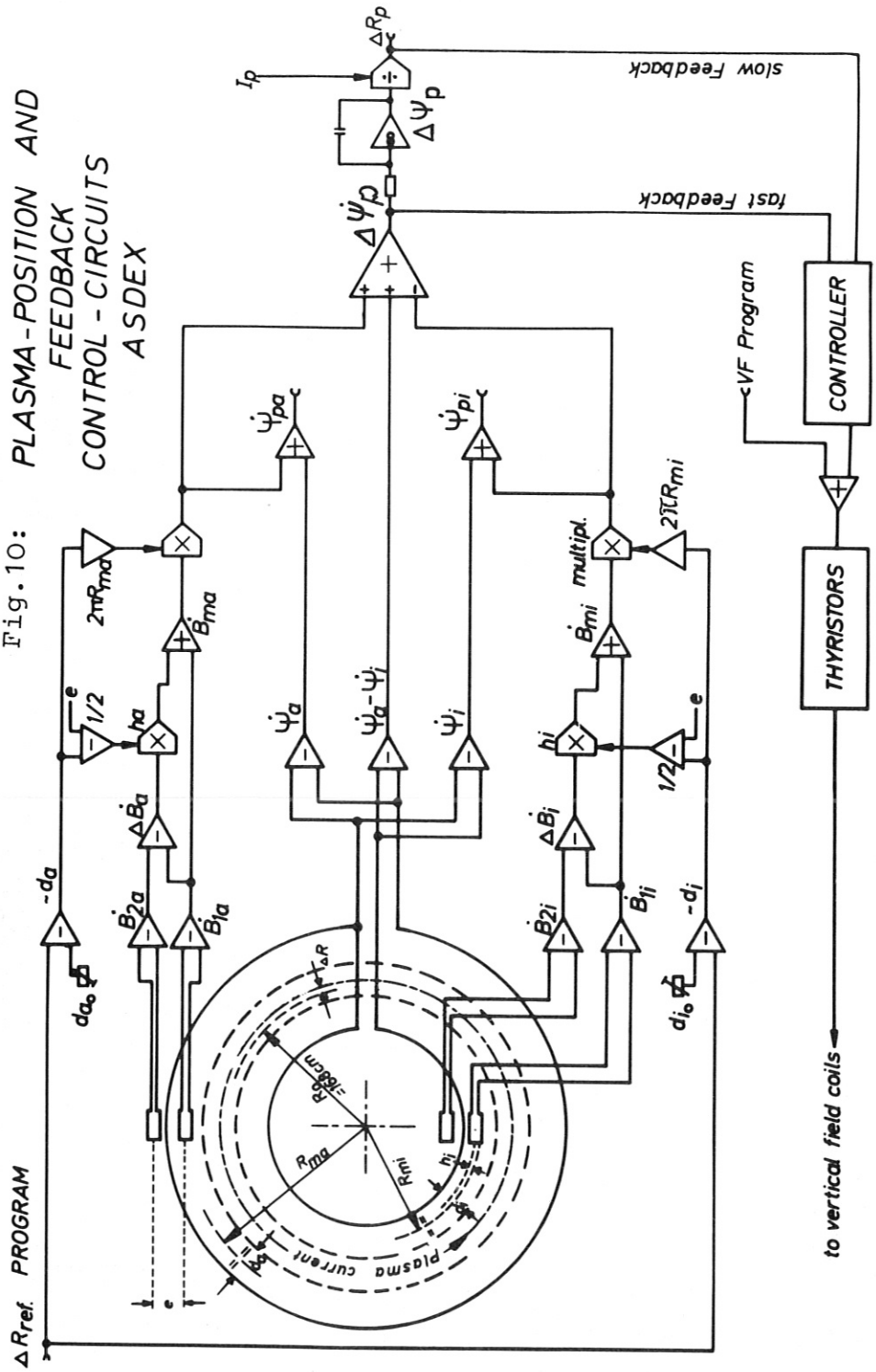
PLASMA-POSITION AND
FEEDBACK
CONTROL - CIRCUITS
ASDEX
PROGRAM
slow Feedback
fast Feedback
VF Program
CONTROLLER
THYRISTORS
to vertical field coils
multipl.
plasma current

Fig.10:

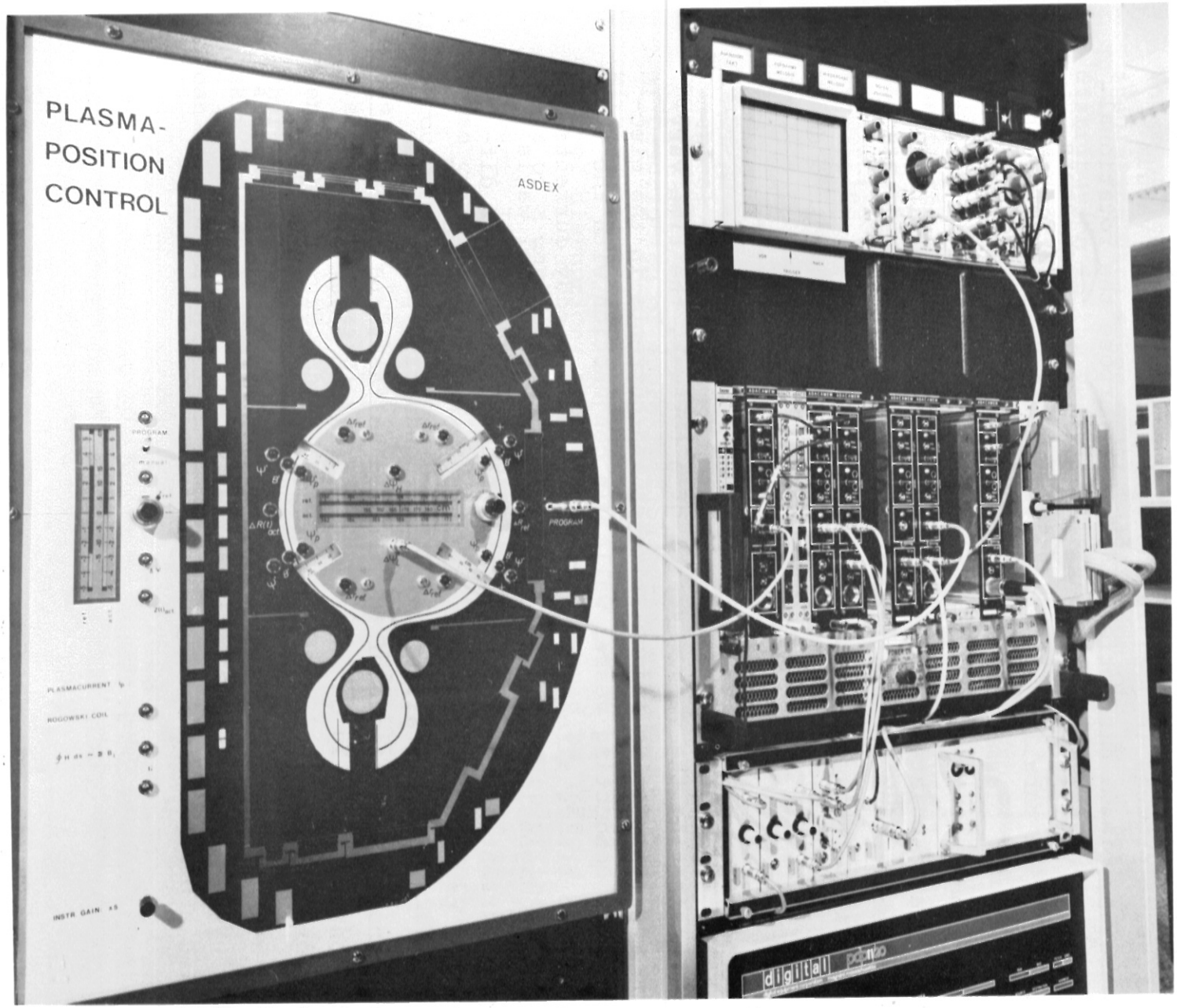

Fig.12 : Central control panel with feedback electronics

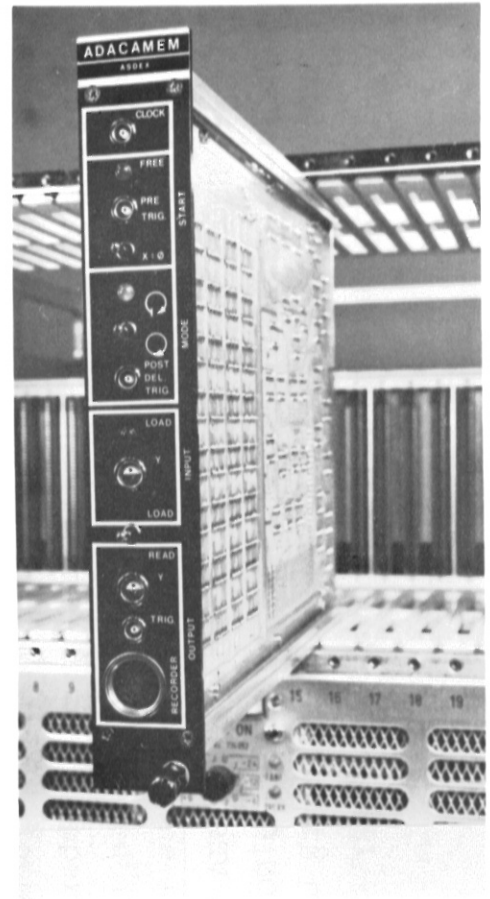

Fig.11: CAMAC module for program control and date acquisition designed for ASDEX feedback system

CALCULATION OF VOLTAGES AND CURRENTS INDUCED IN THE VACUUM VESSEL OF ASDEX BY PLASMA DISRUPTIONS

H. Preis

Abstract:

An approximation method is used to analyze the electromagnetic diffusion process induced in the walls of the ASDEX vacuum vessel by plasma disruptions. For this purpose the rotational-symmetric vessel is regarded as N = 82 circular conductors connected in parallel and inductively coupled with one another and with the plasma. The transient currents and voltages occurring in this circuit are calculated with computer programs. From the calculated currents it is possible to determine the time behavior of the distributions of the current density and magnetic force density in the vessel walls.

Introduction

On penetrating the vacuum vessel of a tokamak, the time varying magnetic fields induce voltages and currents in the electrically conducting vessel walls. In conjunction with the magnetic fields already present the resulting eddy currents produce magnetic forces $\vec{K} = \vec{G} \times \vec{B}$ acting on the vessel walls ($\vec{G}$ = current density, $\vec{B}$ = magnetic flux density). Such diffusion processes, of course, arise not only in the vacuum vessel but also in all electrically conducting parts of the machine. The magnitude of the induced voltages and currents depends essentially on the rate of variation $d\vec{B}/dt$ of the fields. As the fastest field variations are likely to occur in tokamaks owing to plasma disruptions, the diffusion process in the vacuum vessel is to be investigated for this case using ASDEX parameters.

The ASDEX vacuum vessel, which is made of stainless steel sheet, has two electrically insulation gaps. Its meridional cross-section is highly non-circular (see Fig.1).

Figure 1 also shows the size and position of the toroidal plasma column. The divertor cover plates mounted inside the vessel and the attached passive stabilizing copper conductors should be included in the following investigations owing to the small distance between them and the plasma.

The complicated vessel geometry with its installations and insulation gaps makes exact calculation of the current density distribution in the vessel walls very laborious. The same applies to the voltages U_s at the vessel gaps, which are important for assessing the dielectric strength of the insulation materials of the gap. In the long term probably only the finite element method is suitable for numerical solution of this three-dimensional diffusion problem for general vessel geometries /1/. This paper presents an approximation method which can, under certain conditions, provide rather good results.

Numerical calculation

a) Description of approximation method

With negative time variations of the plasma current, as in the case of disruption, toroidal currents would be induced in the walls of a gapless vacuum vessel in the direction of the plasma current. If there are meridional insulation gaps in the vessel, these currents cannot close across the gaps to form toroidal circular currents. They flow in the vessel walls close to the plasma in the direction of the plasma current, and cross over along the vessel gaps to the side furthest from the plasma, hence they return, thus forming a closed circuit. If the discharge times of the plasma current are long relative to the skin time of the vessel, the following method of calculation can be applied:

Starting first with the gapless vacuum vessel, every vessel wall can be approximated in electromagnetic terms by several parallel connected, circular single conductors with rectangular cross-section (see Fig.2). Each conductor can here be characterized by its ohmic resistance self-inductance and its mutual inductances to all other conductors. With N conductors this provides an equivalent circuit composed of N parallel connected, short-circuited branches which are inductively coupled (see Fig.3a, switch s closed) not only with one another but also with the other circuits of the poloidal coil systems (plasma, OH transformer etc.). The equivalent circuit according to Fig.3a now reduces to that in Fig.3b by utilizing the symmetry of the vessel to the horizontal z=0 plane since each of the $n=N/_2$ conductors of the top half of the vessel has the same characteristics $L_{\mu\nu}$ and R_μ as its equivalent conductor in the bottom half. Accordingly one has

$$L_{\mu\nu} = L_{\mu+n,\,\nu+n} \qquad \text{(conductor inductances)}$$

$$L_{p\mu} = L_{p,\mu+n} \qquad \text{(mutual inductances to plasma)}$$

$$R_\mu = R_{\mu+n} \qquad \text{(conductor resistances)}$$

$$I_\mu = I_{\mu+n} \qquad \text{(conductor currents)}$$

for $\mu,\nu = 1(1)n$. These symmetry conditions yield the following relations for calculating the resulting elements (symbolized by ') of circuit 3b:

. Inductances and resistances of the vessel conductors

$$L'_{\mu\nu} = L_{\mu\nu} + L_{\mu,\,\nu+n}$$
$$R'_\mu = R_\mu \qquad \text{for } \mu,\nu = 1(1)n$$

. Mutual inductances between plasma and vessel conductors

$$L'_{p\mu} = L_{p\mu} \qquad \text{for } \mu = 1(1)n$$

. Inductance and ohmic resistance of plasma

$$L'_{pp} = 0.5 \cdot L_{pp}$$
$$R'_p = 0.5 \cdot R_p$$

In the following the influence of the vessel gaps on the equivalent circuit is investigated. It is directly obvious that only breaker s in Fig.3 has to be opened to simulate a meridional insulation gap. After s is opened the current distribution described at the outset is obtained in the vessel, i.e. the currents will flow along the gap in the poloidal direction. It is not certain here what width B (see Fig.1) the cross-over zone at the gap covers. The cross resistance present thus cannot be uniquely determined, this being a basic deficiency of the method. In the case of the ASDEX vessel, however, the resulting error is small because the length of the current path in the toroidal direction is large relative to that in the poloidal direction, thus allowing the cross-over zone to be considered approximately as having zero resistance. As a result the cross resistance between the individual network branches vanish, so that all branches merge in the nodes A and B (see Fig.3). With more than one insulation gap, e.g. m, the equivalent circuit 3 b remains basically unchanged, only the gap voltage U_s assumes the m^{-1}-fold value since the branch impedance also take the m^{-1}-fold value. Of course, the assumption just made ought not to be violated here.

It still remains to describe briefly the mode of operation of circuit 3 b. For the time $t \leq 0$ the stationary nominal current of I_p = 500 kA flows in the plasma. By discontinuous enhancement of the plasma resistance R_p in t = 0 it is possible to simulate a discharge of the plasma current such as would approximately happen in the case of plasma disruption. Here R_p is chosen such that the plasma current I_p has dropped in t_e = 3 ms to 5 % of its nominal value (these data are based on extrapolated experimental results).

The induction processes starting at t = 0 also become effective, of course, in the circuits of the inductively coupled axisymmetric coil system. Their impact there has already been investigated and this is to be published in a separate report. In the context of the vessel current calculation these induction processes are of minor importance and are accordingly neglected.

b) Analysis of the equivalent circuit

In the foregoing the diffusion process was analysed by using the equivalent circuit 3b. Accordingly, the transient currents and voltages in the N network branches are to be calculated with the assumptions made in Sec.a). In order to determine the wall currents and their inversion points P_u (see Fig.1) as exactly as possible, the vessel is divided into N = 82 single conductors (see Fig.2). If a much smaller number N of conductors is chosen, the current density per conductor ought not to be regarded as constant, as is assumed in the method described. The next step is to calculate the inductances between the conductors themselves, and between the conductors and the plasma. This is done with the KOINDUK computer program, which is a revised FORTRAN routine of FORIND /2/. Finally, the transient branch currents and voltages are calculated with the ECAP /3/ or RLNETZ computer programs taking all inductive couplings into account. Both routines are based on the solution of a system of M-dimensional network differential equations /4/, the version of ECAP installed at the IPP Computing Centre admitting a maximum of M=45. Accordingly, the newly developed RLNETZ routine was used for systems of differential equations with $M \geq 45$.

Representation of results

Figure 4 shows the time behaviour of the resulting vessel currents I_{go} and I_{gm} (sum of all currents flowing in the direction of the plasma current) during plasma disruption for 3 ms, compared with the plasma current I_p. Here I_{go} was calculated for a vessel without insulation gap, and I_{gm} for a vessel with two insulation gaps. Providing insulation gaps reduces the maximum of the induced currents from 48 % to 27 % of the plasma current. If the diffusion process is regarded as complete when the vessel currents have dropped to e^{-1} of their maximum value, the diffusion time for I_{gm} is t_d = 28.6 ms (see Fig.4).Also shown in Fig.4 is the time behaviour of the voltage U_s at the insulation gap of the vessel.

In Figure 5 the toroidal current density prevailing at time $t=t_m$ (see Fig.4) in the walls of the vessel with gaps is plotted versus the rectified coordinate s along the circumference (see Fig.2). The current density is positive when it has the same direction as the plasma current.

From the magnitude and direction of the toroidal currents it is easy to determine the currents I_s crossing over along the gap (see Fig.5). They flow perpendicularly to the toroidal field of approximately 3 T and thus produce in the walls of the ASDEX vessel force densities of up to $\vec{K}$ = 2000 N/cm, whose effect was analyzed in /5/.

Finally, it should be mentioned that measurements with the same objective were made in an ASDEX model (scale 1:10) /6/. Comparison of the measured and calculated results yielded a large degree of agreement. In conjunction with /5/ and /6/ the investigations described have had a major influence of the designing of the ASDEX vacuum vessel.

References

/1/ J.Donea, S.Giuliani, A.Philippe: FiniteElements in the Solution of Electromagnetic Induction Problems. Int.J.for Num.Meth.in Engineering, Vol.8 (1974).

/2/ R.Pöhlchen: Calculations of self-inductances of thick aircore coils, mutual inductances and axial forces between such coils in coaxial systems by means of digital computer. IPP-Report 4/93, 1971

/3/ IBM: Electronic Circuit Analysis Progr. II (ECAP II) for the IBM Operating System an 1130 Computing System Progr. Description Manaul. Progr.Numbers 5734-EE1, 5711-EE1.

/4/ H.Preis: The analysis of transient pheomena in linear electric networks (in German). IPP-Report 4/87, 1971.

/5/ O.Jandl, H.Kotzlowski: Stress Analysis of the Vacuum Vessel of ASDEX, Proc.10th SOFT, 1978, Padova, Italia

/6/ F.Schneier: Private message of measuring results.

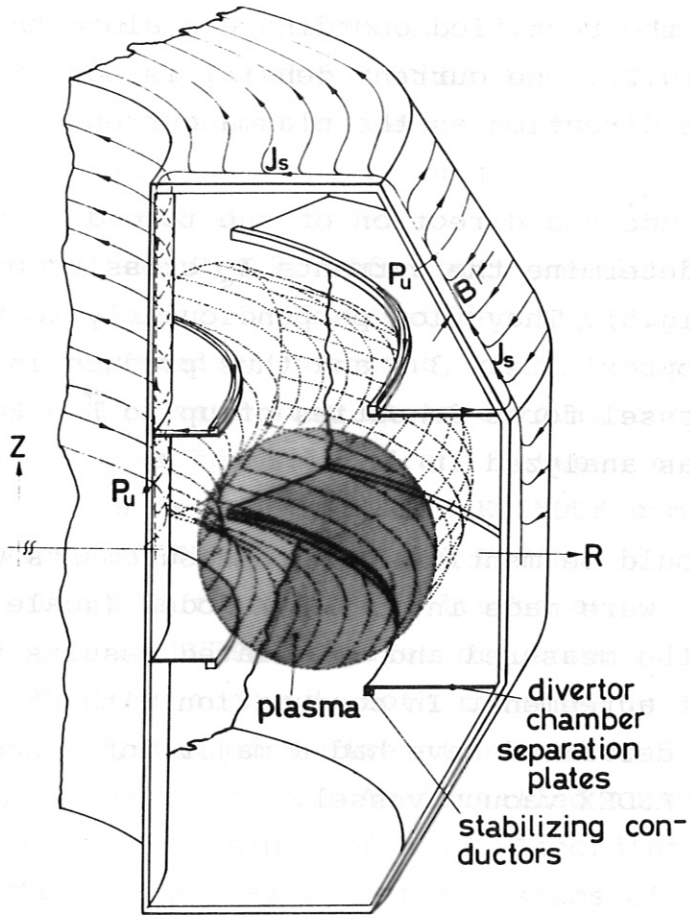

Fig.1: ASDEX-vacuum vessel

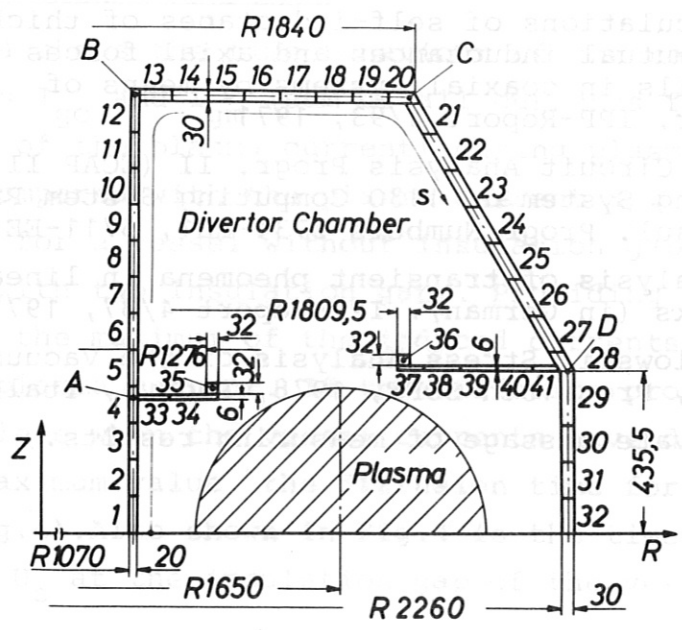

Fig.2: Meridional cross-section of vessel showing conductor arrangement.

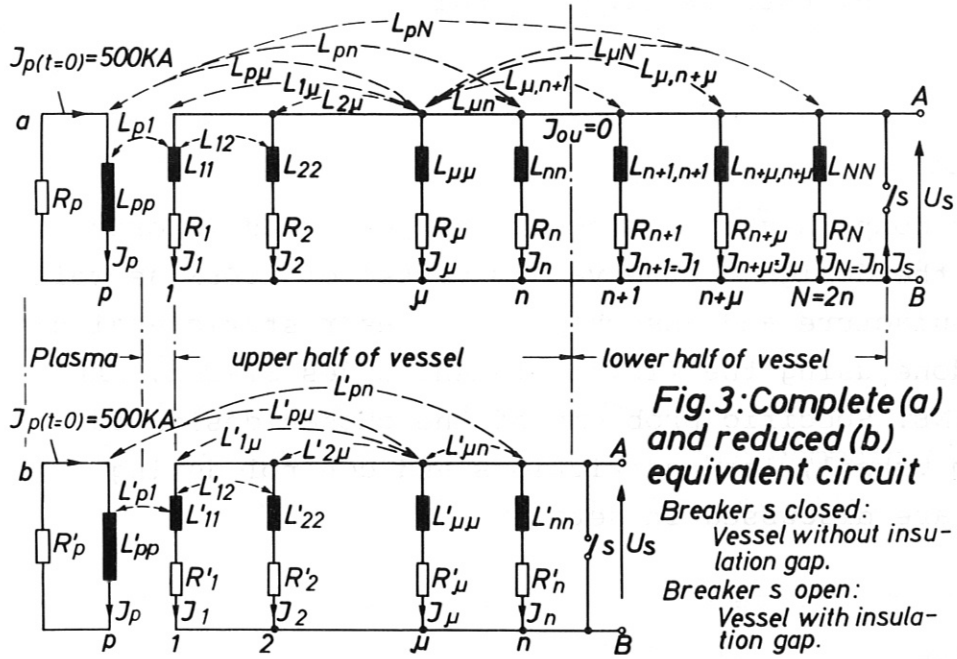

Fig.3: Complete (a) and reduced (b) equivalent circuit

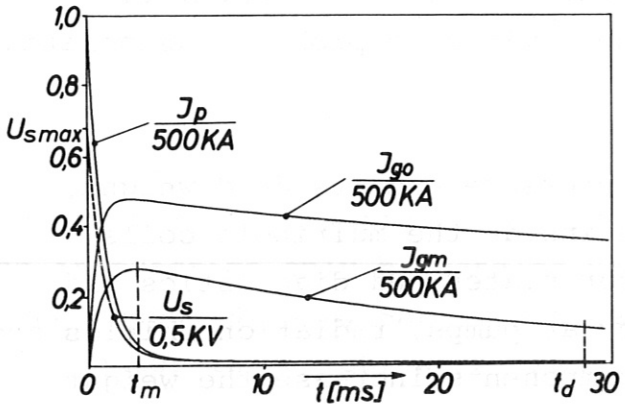

Fig.4: Time variation of current and voltage at the gaps.

J_p plasma current

J_{go} current in vessel without gap

J_{gm} current in vessel with gap

U_s voltage at gap.

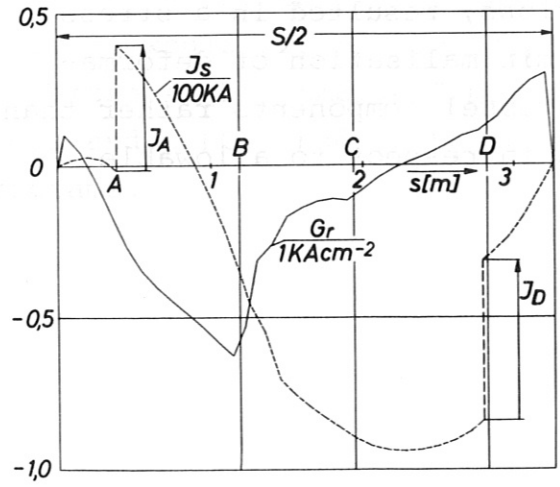

Fig.5: Current distribution in vessel with two gaps at time t_m of maximum current.

S rectified poloidal length of circumference

Gr toroidal current density

Js poloidal current along gap

J_A, J_D currents in divertor chamber separation plates

STRESS ANALYSIS OF THE VACUUM VESSEL OF ASDEX

H. Kotzlowski, O. Jandl

Abstract:

This paper comprises the calculations performed in order to establish the design of the vacuum vessel of ASDEX as well as its manufacture and assembly. The linear static analysis has been done using the finite element codes STRUDL, SAP and STARDYNE. Specific problems of the chosen design for the vacuum vessel, its restrictions and control during operation are discussed in detail.

Introduction

The construction and technology of the vacuum vessel of ASDEX have gained a lot from the experience made on PULSATOR, and thus new developments could be limited to problems associated with size and shape.

The vessel, stressed by atm. pressure and its dead weight, supports and positions on the inside the multipole coils, Ti-sublimation pumps, collector plates and diagnostics and on the outside the turbomolecular pumps, radiation shields and external diagnostics. These components increase the weight of the vessel from 18 to 32 t. A requirement for high rigidity of the vessel structure, as well as a preservation of flexibility for operational modifications, resulted in a stress analysis that concentrates on a minimalisation of deformation and reaction forces to the vessel components rather than on an optimisation of the design in respect to allowable stresses.

Design of the vacuum vessel

In principle the vessel consists of a toroidal shell of 20 mm (inner cylinder) and 30 mm (rest of the shell) thickness. 218 ports in sizes of 35 mm to 600 mm in diameter and of Conflat type are placed in the 30 mm thick part of the wall (Fig.1). For assembly the torus is splitted in its vertical plane. The two gaps are reinforced by 40 mm thick and 90 - 160 mm high flanges and bolted together from inside the vessel. On the outside, the parting flanges are linked together across the gap via reinforcing plates. Between the parting flanges a 10 mm thick polyimid frame composed from 20 parts - as no larger pieces of this material are commercially available - insulates the vessel halves electrically.

The outer surface of the vessel is equipped with heating pipes for baking up to 150^{o} C by overheated water and thermally insulated with foamed silicon rubber. The vessel is supported by eight toroidal field coils and adjustably positioned by a cantilever linked to the foundation of ASDEX /1/.

Stress analysis

The analysis of elastic behaviour of the vacuum vessel of ASDEX can in practice only be handled using a finite element program. Three codes: STRUDL, SAP (installed at Garching) and STARDYNE (CDC-center in Munich) were used for the discussed analysis.

Representation of the complete vessel structure by one mesh of finite elements - taking advantage of symmetry and antimetry - would exceed the computational capacity available. Therefore eight "smaller" meshes (up to 1100 elements, 1350 nodes and 5 DOF) had to be generated, mainly by self-written programs.

Inner diameter	2140 mm
Outer diameter	4580 mm
Height	2430 mm
Wall thickness	20 and 30 mm
Volume	26 m^3
Internal wall area	67 m^2
Weight (structure only)	18 000 kg
Weight (during operation)	32 000 kg
Materials	
- Vessel	AISI 304 LN
- Electrical insulation	Vespel Sp1 10 mm
- Thermal insulation	foamed silicon rubber 15 - 25 mm thick

Parameters of the vacuum vessel of ASDEX

a) Additional weight and atm. pressure

The maximum stressing of the shell due to the above loading occur in the top and bottom plates of the vessel. As the max. stresses of 55 N/mm^2 and deformations up to 0.4 mm are relatively low, a reinforcement of the vessel through poloidal ribs was abandoned in favour of a more simple manufacture and flexibility for operational modifications - however at the expense of the assembly.

Calculations were performed for manufacture, assembly and transport in order to minimise the distortions and reaction forces within the vessel components as an unfavourable clamping or support would endanger the required tolerances an the fit of the vessel halves.

b) Thermal load

During the baking-cycle the vessel undergoes a nonuniform temperature change, formed mainly by gradients in the wall and along the poloidal circumference. Gradients, normal to

the wall, are caused by the low thermal conductivity of stainless steel and the poor thermal flux to the divertor components via bolted connections. The established slow heating- and cooling speed of 10° K/h reduces these temperature differences of the wall surfaces to approx. 8° K. However, more problematic is here the temperature variation along the poloidal circumference. The variation, measured on a model (up to 18° K), and put into a 3D-calculation, results in high forces at the screw joint which stress the electrical insulation considerably (Fig.5). The remaining prestress at the bolts - inevitable for the vacuum seal - reaches its minimum in the middle of the inner cylinder, where the height of the parting flanges is reduced.

c) Multipole forces

Under normal operation of ASDEX the electromagnetic forces, acting at the multipoles, are being compensated within a triplet. To induce a non-circular plasma only the MP2 coils are to be energised,whereby they attract each other with 680 kN /3/. Induced stresses of 103 N/mm^2 in the top plate, and deflections of up to 1.6 mm are tolerable neither for the vessel nor for the coils. Therefore, the multipole coils have been fixed at the divertor plates, which are supported by the inner cylinder and the cones (Figs. 2,3 and 4).

d) Plasma disruption

The poloidal eddy currents along the gaps of the vessel at plasma disruption - measured on a model of ASDEX (Fig.6) /1,4/ and confirmed by numerical calculations /5/ - generate antimetric electromagnetic shear forces at the screw joints of the vessel halves (Fig.7). As their toroidal distribution is not known, assumptions had to be made for the calculation.

The maximum stressing of the shell occur when the forces are toroidally distributed over a segment of 6^{o} (measured from the middle of the gap). Figure 8 shows the stress variation in section 1 (weld-joint to the parting flange), in section 4 (4^{o} from the gap) and in the parting flange. Due to the high rigidity of the parting flanges the stressing is here more independent of the distribution of the forces than in the shell. However, their shift at the inner cylinder (Fig.10) of 2 x 0.4 mm= 0.8mm creates new problems, still under investigation, associated with the lifetime of the Viton-O-rings.

Conclusions

The most problematic part of the chosen design for the vacuum vessel of ASDEX is the screw joint at the electrical insulation of the vessel halves. Here already the temperature variation during baking and the electromagnetic forces at plasma disruption generate critical stresses and deformations which must be monitored during operation. The measurements comprise the

- temperature distribution in the shell
- vertical forces at the eight supports of the vessel
- relative displacement of the parting flanges in its vertical plane
- distance of the parting flanges
- prestress at four bolts per screw joint.

References

/1/ The ASDEX Group: "Divertor Tokamak ASDEX", IPP Report III/27 (1976)

/2/ S.Timoshenko: "Theory of Plates and Shells", McGraw Hill, (1959)

/3/ M.Pillsticker et al.: "Technical Concept for the Multipole Coils of ASDEX", Proc. 9th Symp. on Fusion Technology, Garmisch-Partenkirschen, 1976

/4/ F.Schneider: private communication

/5/ H.Preis:" Calculation of induced voltages and currents in the vacuum vessel of ASDEX in the case of Plasma Disruption", Proc. 10th Symp. on Fusion Technology, Padova, 1978.

Legend to Fig.1:

1 Inner cylinder
2 Top plate
3 Top cone
4 Outer cylinder
5 Bottom cone
6 Bottom plate
7 Supporting plates
8 Parting flange
9 Screw joint
10 Reinforcing plates
11 NW 600 port (manhole)
12 NW 350 port (diagnostics)
13 NW 300 port (pumping)
14 NW 180 port (multipole coils)
15 Electrical insulation
16 Fixing fillets for divertor components

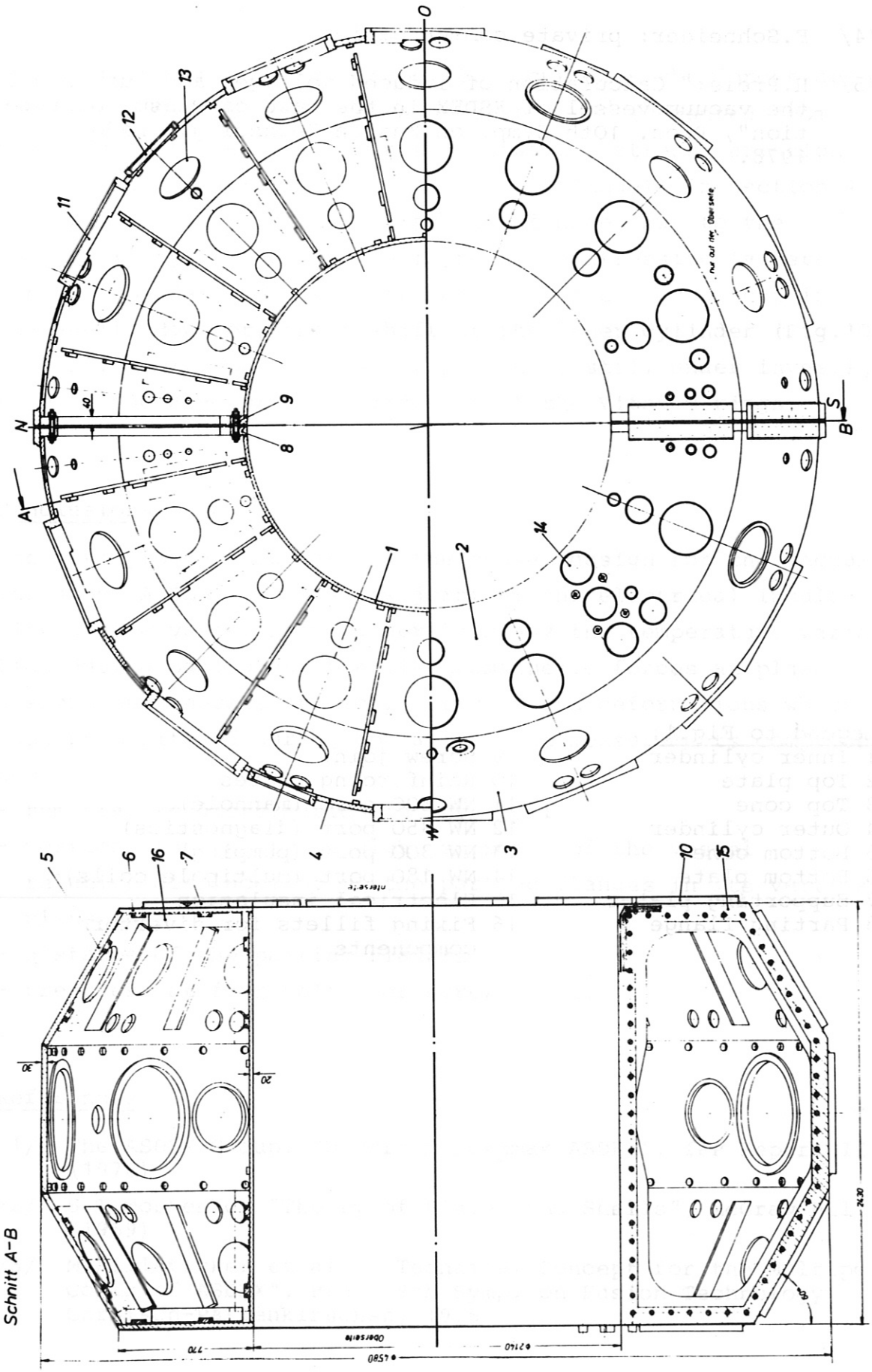

Fig.1: Vacuum vessel of ASDEX - plan and elevation section views

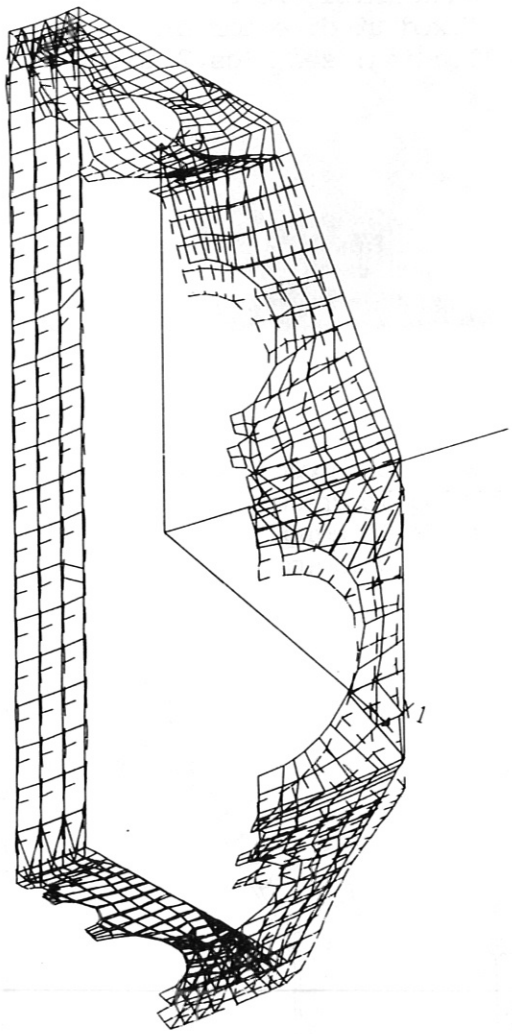

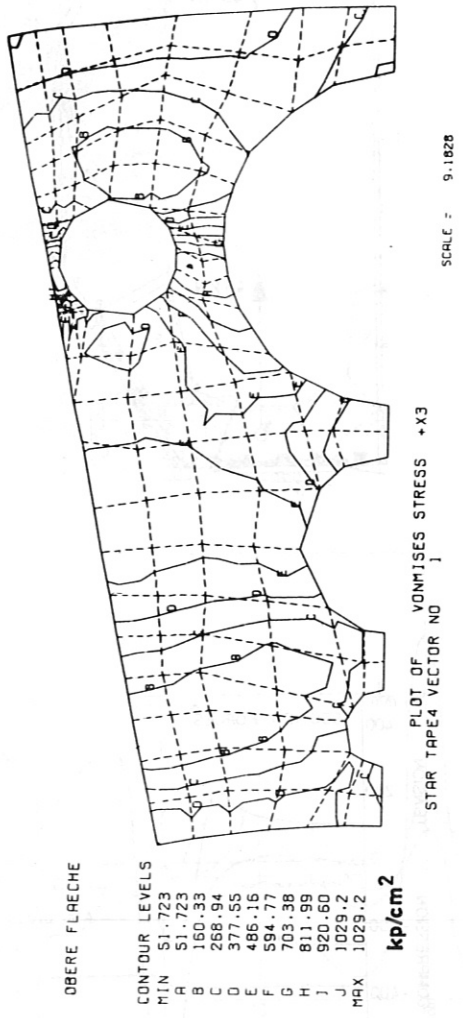

Fig.2: Deformation of vessel segment
max. z = 1.6 mm

Fig.3: Stresses (von Mises) in top plate of vessel segment

loading: additional weight + atm. pressure + multipole forces (noncircular plasma operation) multipoles fixed at top and bottom plates of the vessel.

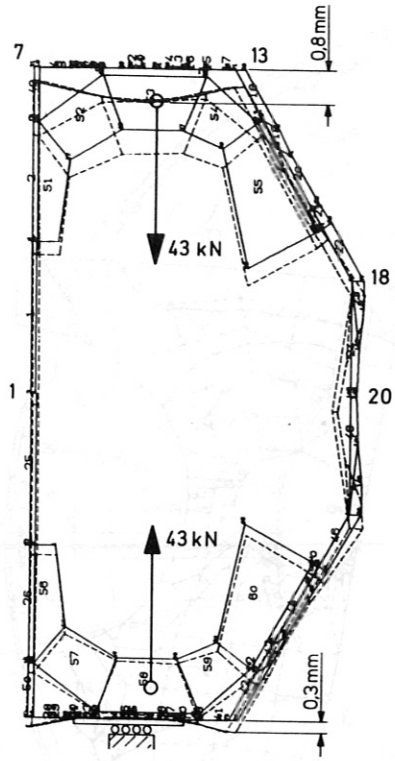

Fig.4: Deformation of the vessel when multipole coils are fixed at divertor plates loading: see Figs.2 and 3

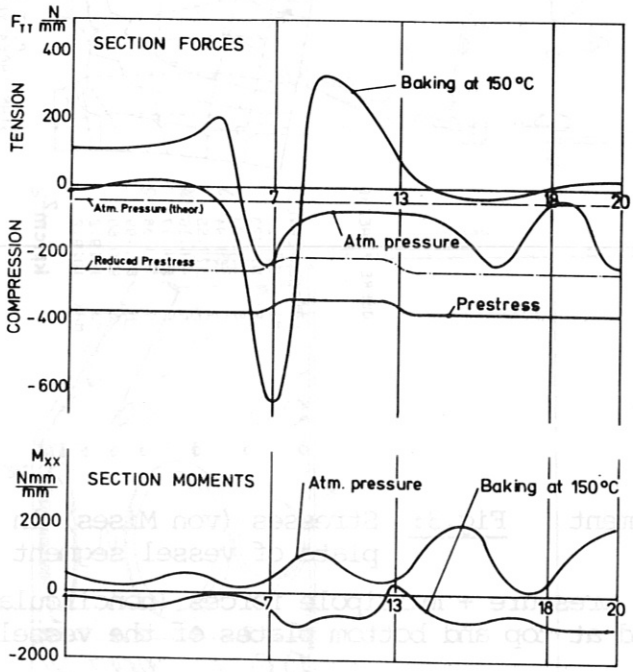

Fig.5: Stresses (von Mises) in the shell and section forces at screw joint of the vessel.

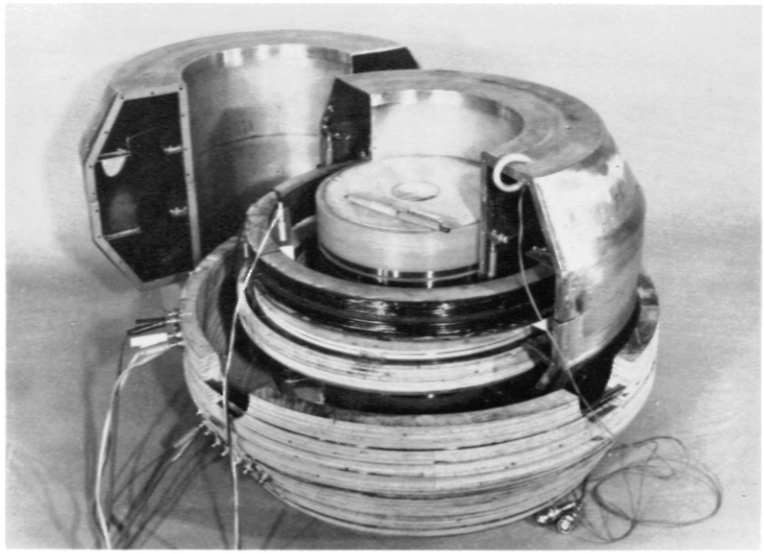

Fig.6: Model of ASDEX (scale 1:10) for measurement of poloidal eddy currents along the gaps of the vacuum vessel at plasma disruption /1,4/

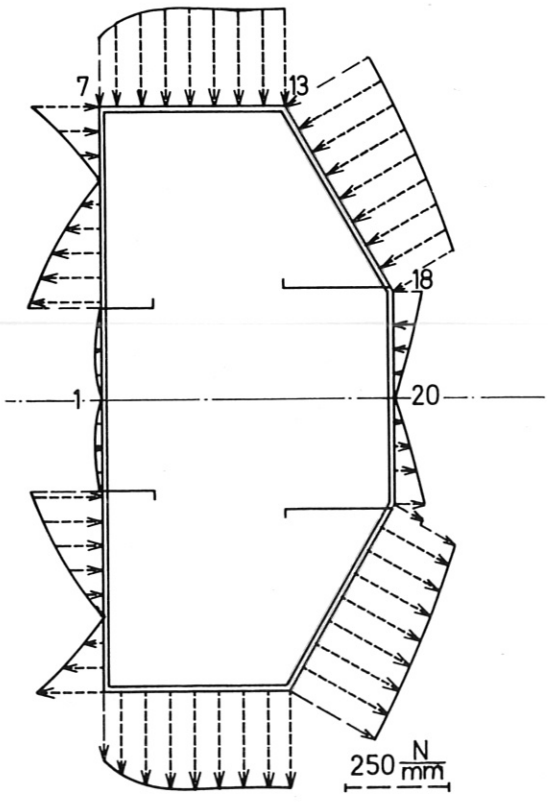

Fig.7: Electromagnetic forces acting on the vessel at plasma disruption in 3 ms /5/

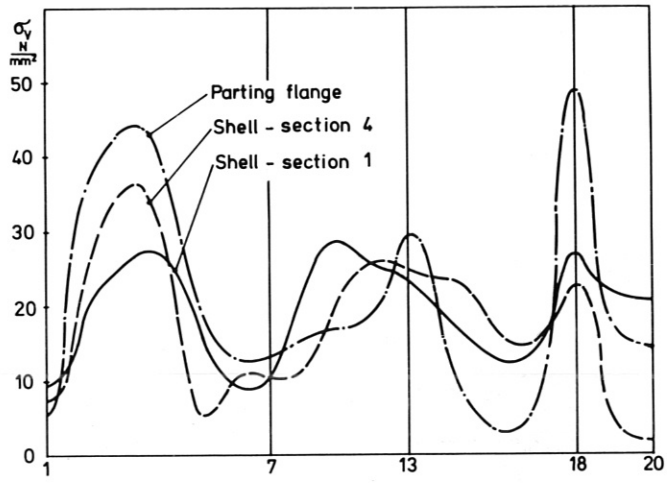

Fig.8: Stresses (von Mises) in the shell and parting flange of the vessel at plasma disruption in 3 ms

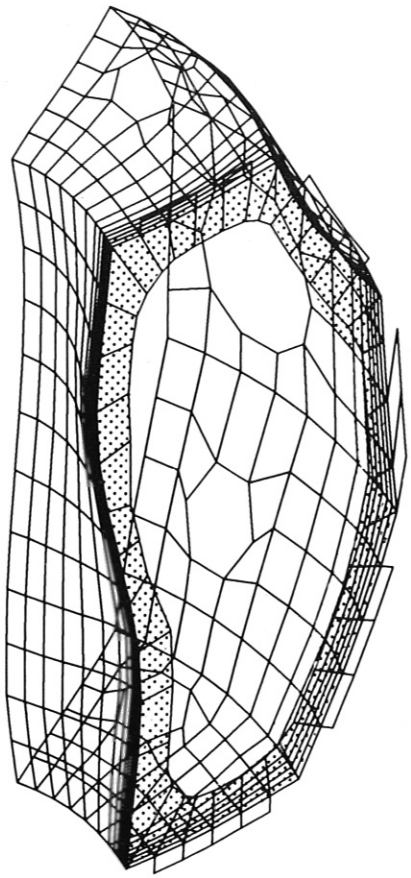

Fig.10: Deformation of the parting flange and shell of the vessel at plasma disruption in 3 ms max. R=0.4 mm.

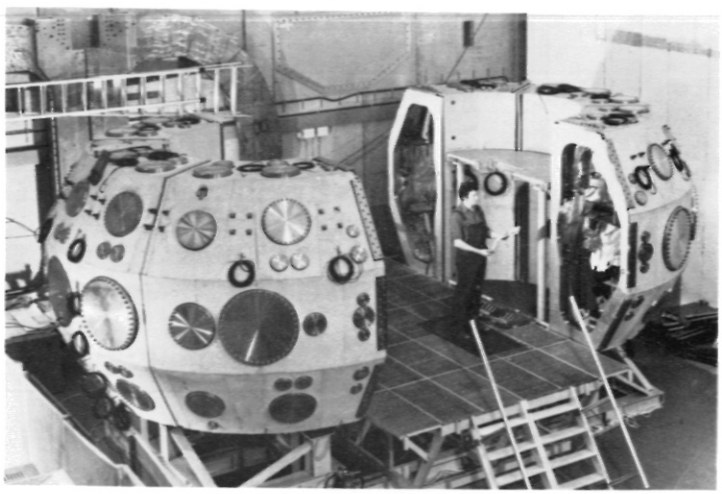

Fig.9: Vacuum vessel of ASDEX - installation of divertor, diagnostics and control components.